CDF/ANAL/EXOTIC/CDFR/10559
Version 2.0
July 3, 2011

Improving WH Neural Network Analysis Using Loose Electron-Like Leptons

Weiming Yao (LBNL)
for the WH Working Group

Abstract

We present a new selection of W events to be used in the $WH \to l\nu b\bar{b}$ analysis. The new events are selected by requiring a high P_T track with significant deposits of energy in the calorimeter that are primary from the decay of $W \to e\nu$ or $\tau\nu$ where the electron failed the standard electron selection or the τ decays into a single charged hadron (one-prong). We search for $WH \to l\nu b\bar{b}$ candidate events with two jets, large $\not\!\!E_T$, and exactly one loose electron-like lepton candidate from the inclusive electron trigger and the missing energy trigger. We present the analysis technique used for these new events that results a gain of 30% more electrons in the acceptance of WH events. This new analysis selection is applied to the data through period 34, corresponding to an integrated luminosity of 7.5 fb^{-1}. We find $\sigma(p\bar{p} \to W^{\pm}H) \times \mathrm{Br}(H \to b\bar{b})$ with an observed limit 7.9 $\times$ SM prediction (9.3 expected) for $m_h = 115$ GeV/c^2 at 95% confidence level. When combining with the existing WH channels, the WH sensitivity is improved an average of 5.6% for $100 \leq m_h \leq 150$ GeV/c^2.

1 Changes in V2.0

We made few improvements to the current analysis that are summarized below.

- Measured loose electron identification and scale factors as a function of electron E_t.
- Improved non-W model for loose electron by requiring electron likelihood < 0.1.
- Added extra $Z \to ee$ removal.
- Rescaling Q*η of loose muon to match with the looser isolated track in 1jet bin.
- Quantified the impact of overlap with other channels is small up to 1%.

2 Introduction

This note describes an improvement to the existing search for $p\bar{p} \rightarrow WH \rightarrow \ell\nu b\bar{b}$ in events that have at least one SECVTX b-tagged jet. The improvement consists of including two types of loose electrons to the standard W selections. The first type is "Loose CEM", selected using a multivariate electron likelihood method from the high P_T central electron triggers and the second type is "ISOTKh", selected from the missing energy trigger by requiring an isolated track with significant deposits of energy in the calorimeter. In the existing analysis, the lepton was required to be identified as either an electron (CEM, PHX), a muon(CMUP, CMX), or an isolated track with an energy deposit in the calorimeters consistent with that of a minimum-ionizing particle. These new events are primary from the decay of $W \rightarrow e\nu$ or $\tau\nu$ where the electron failed the standard electron selection or the τ decays into a single charged hadron (one-prong).

Treating these new lepton types as independent channels, we go through the full analysis procedure,including b-tagging, forming an event discriminant, and setting limits on the WH production cross section. These limits will be used in combination with the full $WH \rightarrow l\nu b\bar{b}$ analysis, as well as with other channels.

3 Data Samples and Event Selection

The data used for this analysis come from the high P_T inclusive central electron trigger (`bhel`) and the $\not\!\!E_T$ dataset (`emet`), which were collected through March 2011. The first part of data from period 0-17 were processed using the production software 6.1.1 and the second part from period 18-34 were processed using the production software 6.1.6p+. We select events with no tight leptons reconstructed, but containing either a loose CEM electron from bhel trigger or a high-p_T isolated track that is required to pass one of the following MET triggers:

- `MET35_&_TWO_JETS`
- `MET35_&_CJET_&_JET`
- `MET35_&_CJET_&_JET_LUMI_190`
- `MET35_&_CJET_&_JET_DPS`
- `MET45(MET40)`

We use a $\not\!\!E_T$ + jets (MET2J) and $\not\!\!E_T$ trigger (MET45) parallel and will describe details in the event selection section.

Our Higgs signal model comes from the official Higgs Discovery Group Higgs Monte Carlo (MC) samples generated with PYTHIA using the standard MC procedure outlined in CDF software version 6.1.4. These Higgs samples were generated for a range of Higgs masses from 100 GeV to 150 GeV. Our background models are composed of

a number of components. The W and Z plus light-flavor and heavy-flavor jet processes are modeled using ALPGEN version 2.10 showered with PYTHIA. Likewise, the single-top contribution is modeled using parton-level events generated by MadEvent and showered through PYTHIA. The rest of the background processes, including the $t\bar{t}$, WW, WZ, and ZZ processes were generated with PYTHIA. For backgrounds involving a top quark, the top mass was set to 172.5 GeV/c^2.

3.1 Luminosity

We use the standard luminosity calculation provided by the top group including corrections for trigger prescales on a run-section by run-section basis. This calculation uses version 40 of the DQM silicon good run list (bits [1,1,4,1]) for data through period 34. The luminosity for the bhel triggered events is 7.5 fb^{-1}. The luminosity for the MET2J triggered events is 7.0 fb^{-1}. The luminosity for the MET45 triggered events is 7.5 fb^{-1}.

3.2 Event Selection

Loose Electron Event Selection We improve the standard electron selections of the existing $WH \to l\nu b\bar{b}$ analysis [1] to select additional $W \to e\nu$ events from the high P_T inclusive electron trigger (`bhel`) using a multivariate electron likelihood method that developed by the $H \to W^+W^-$ search group [2]. A selected electron candidate is required to pass the following selections:

- Electron Likelihood > 0.9, but failed the tight electron cut
- $E_T > 20$ GeV
- $|Z_0| < 60$ cm
- not tagged as conversion
- Isolated in Calorimeter as $Iso < 0.1$
- Apply single-top QCD veto to reduce the non-W background
- Pass dilepton and extra $Z \to ee$ veto

There is a potential gain of 20% more electrons with the new selection in WH115 Monte Carlo, mainly due to relax of the fiducial requirement. There are also more non-W background that can be reduced by requiring the standard single-top QCD veto. Since these electrons could come from outside the CEM fiducial region, we have to measure the correspond trigger efficiency and a possible scale factor for electron identification mismatch between data and Monte Carlo. The trigger efficiency is found to be 0.903 ± 0.003 using $Z \to e^+e^-$ events where the tag electron is in the Plug region and the prob electron is in the central region, which is expected to be bit lower than

the electron passing the standard cuts (0.961 ± 0.001). The scale factor (SF) of electron identification is found to be 0.983 ± 0.008, which is consistent with the tight electron. Figure 1 shows the trigger efficiency as a functionof electron E_T, which seems relative flat. Figure 2 shows the electron identification efficiencies in the data and Monte Carlo and their corresponding scale factor that is used to correct for the Monte Carlo events.

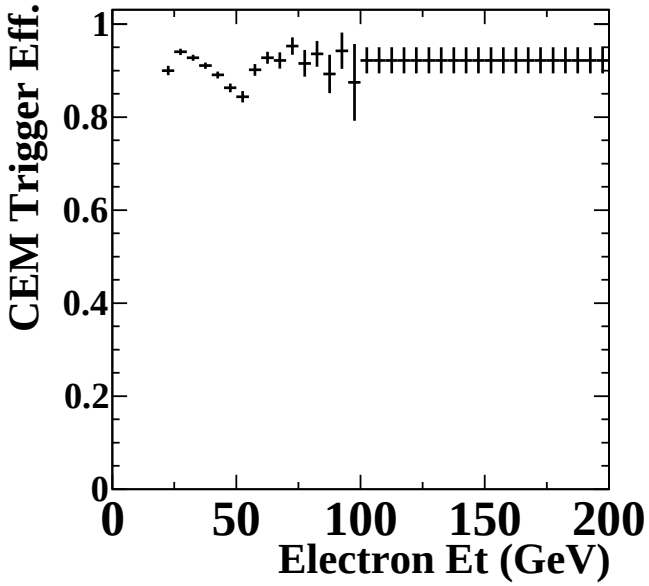

Figure 1: The CEM trigger efficiency for loose electron is shown as a function of electron E_T.

Looser Isolated Track Event Selection We improve the isolated track selections of the existing $WH \to l\nu b\bar{b}$ analysis [1] to select additional $W \to e\nu$ or $W \to \tau\nu$ events from the $\not\!\!E_T$ triggers where the electron failed the standard electron identification or the τ decays into a single charged hadron (one-prong). We use the same selection criteria described in the previous analysis [3] that are summarized in Table 1 to select high quality, high-p_T isolated tracks (ISOTKh) with $|\eta_{track}| < 1.2$ and a significant energy deposit in the calorimeter as a tight jet. We use a variety of vetoes to ensure that isolated tracks events are from W events and that they do not overlap with other lepton identifications.

- **Two Track Veto**: We count the number of isolated tracks in the event. If there are two or more isolated tracks, we veto the event.
- **Extra Z removal**: We remove the events if any of two opposit-signed high p_T tracks has an invariant mass within the Z mass window between 76 and 106 GeV/c^2.

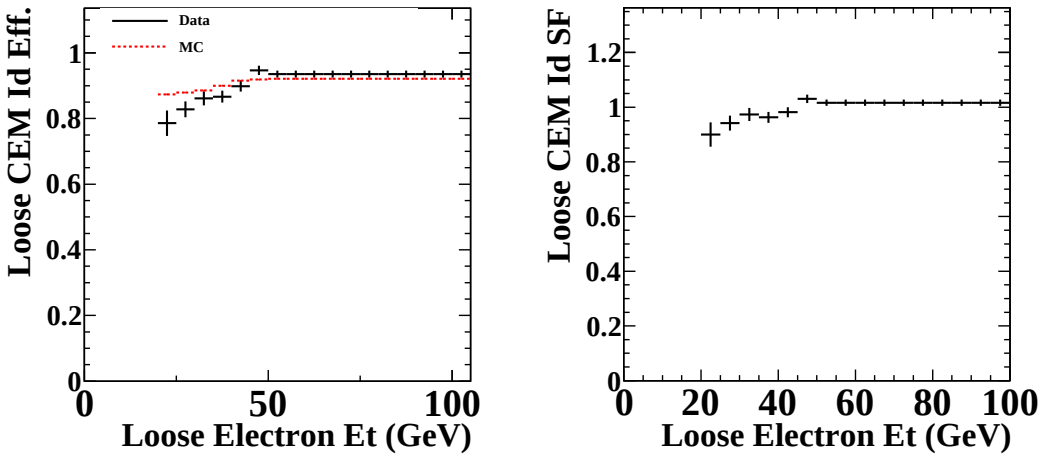

Figure 2: The electron ID efficiencies for loose electron are shown in data and Monte Carlo (left) and their corresponding scale factor as a function of electron E_T (right).

- **Standard Lepton and Isolated Track Veto**: If the event contains any identified lepton or an isolated muon-like track (ISOTKm) that used in the standard WH analysis, the event is not allowed to pass the ISOTKh selection.
- **Hadronic Isolation<5%**: The track is required to be isolated in the hadronic calorimeter (Hadiso) to be consistent with an electron or one-prong hadronic τ decay where the Hadiso is defined as the ratio of sum of energy deposits in the surrounding towers in the hadronic calorimeter over the track p_T.
- $\not\!\!E_T$ **not pointing to any tight jet excluding the lepton-jet**: The $\not\!\!E_T$ is required to not point to any jet $\Delta R > 0.4$.
- **QCD veto**: A cut of $m_T^W > 10$ GeV is required to suppress the non-W background contribution.

The $\not\!\!E_T$ is corrected for the presence of muons (including muon-like isolated tracks) and jet energy corrections (JES). The jets are identified using the JetClu algorithm with a cone of 0.4 and are required to be central ($|\eta_{Det.}| < 2.0$) with $E_T > 20$ GeV, corrected for level-5 jet corrections.

3.3 Jets Trigger Requirements

The MET2J trigger has been used extensively at CDF and has shown that that the trigger's jet requirements are fully efficient after the following cuts:

- Two Tight Jets with $E_T > 25$ GeV

Variable	Cut
p_T	> 20 GeV
$\|z_0\|$	< 60 cm
$\|d_0\|$corr	< 0.2
$\|d_0\|$corr (w/SI)	< 0.02
track isolation	> 0.9
Axial COT hits	≥ 24
Stereo Hits	≥ 20
χ^2 probability (data only)	$> 10^{-8}$
Num Si Hits (data only, only if num expect ≥ 3)	≥ 3
Matching to a jet	$\Delta R < 0.4$
TrkIsol($\frac{P_T^{cand}}{P_T^{cand}+\Sigma P_T}$)	> 0.9

Table 1: Looser Isolated track selection cuts

- $\Delta R > 1.0$
- One central jet with $|\eta| < 0.9$

We apply these additional jet cuts after identifying the tight jets in the event. For events with 3 or more jets, we require that the two lead jets in the event satisfy these requirements. If any one of the MET2J trigger-related requirements above failed, we consider that event as part of an orthogonal sample which requires the MET45 trigger.

We use the parameterization of the MET2J and MET45 trigger turn-on curves for each trigger level separately as a function of level-5 jet corrected vertex $\not\!\!E_T$ that measured using the inclusive CMUP trigger [4]. We choose level-5 jet corrected vertex $\not\!\!E_T$, which is corrected for the primary vertex position and takes into account the level-5 jet energy correction but not corrections derived from muons.

3.4 *b*-Tagging

We adopt the *b*-tagging strategy that used in the standard WH analysis [1], which maximizes the number of events with two or more *b*-tags by making use of the SecVtx, jet probability (5%), and RomaNN algorithms. Every event with at least one SecVtx *b*-tagged jet falls into one of four exclusive tag categories, defined below:

SecVtx **tight** + SecVtx **tight (STST):** Events in this category are required to have both jets tagged by the tight operating point of SecVtx.

SecVtx **tight + Jet Probability 5% (STJP):** Events in this category are required to have one jet tagged by the tight operating point of SecVtx and one jet to be tagged by the jet probability algorithm. To be tagged, a jet must have a jet probability of less than 5%.

SECVTX **tight + RomaNN (STRoma):** Events in this category are required to have one jet tagged by the tight operating point of SECVTX and one jet to be tagged by the RomaNN algorithm. To be tagged, a jet must have an output value greater than 0.0.

SECVTX **tight (SST):** Events in this category are required to have exact one SECVTX tight tagged jet and with no additional SECVTX, jet probability or RomaNN tags.

In order to further improve the b-tagging purity for the events containing only one SECVTX b-tagged jet, we also include the Karlsruhe Neural Network b-tagger (Kitnn) as a b-jet discriminant from light flavor or charm quarks which uses jet characteristics as well as secondary vertex information [5].

3.5 Neural Network b-jet Energy Correction

The most sensitive variable for WH analysis is the dijet invariant mass. Improvement on dijet mass resolution directly results in improvement of the final sensitivity. To further improve the dijet mass resolution, a neural network based b-jet energy correction method was developed [6]. We employ four neural network functions for each b-tagging type: SECVTX, JP, RomaNN, and not-tagged.

3.6 Neural Network Discriminant

To further improve signal-to-background discrimination after event selection, we employ a Bayesian neural network (BNN) [7] trained on a variety of kinematic variables to distinguish WH from backgrounds. One advantage using BNN is less prone over-training because of the bayesian sampling.

For this analysis, we use the same BNN discriminant functions that are optimized for the central lepton and one of three tagging categories: STST, STJP and STRoma, and SST [1].

3.7 Looser Isolated Track Modeling

In order to check how well the loose isolated track selection modeled in the Monte Carlo, we select the events containing one tight central lepton and one isolated track with a large missing$\not\!\!E_T > 20$ GeV. The opposite-sign pair with back-to-back provides a clean sample of Drell-Yan that can compare directly to the Monte Carlo shape. Lots of work has been done in the tight isolated track analysis. The only thing we need to check is addition jet requirement and Hadiso cut. Figure 3 shows matched jet E_T, η, ΔR between the track and matched jet, $\Delta\phi$ between track candidate and$\not\!\!E_T$, and Hadiso, respectively. Overall, the agreement is excellect.

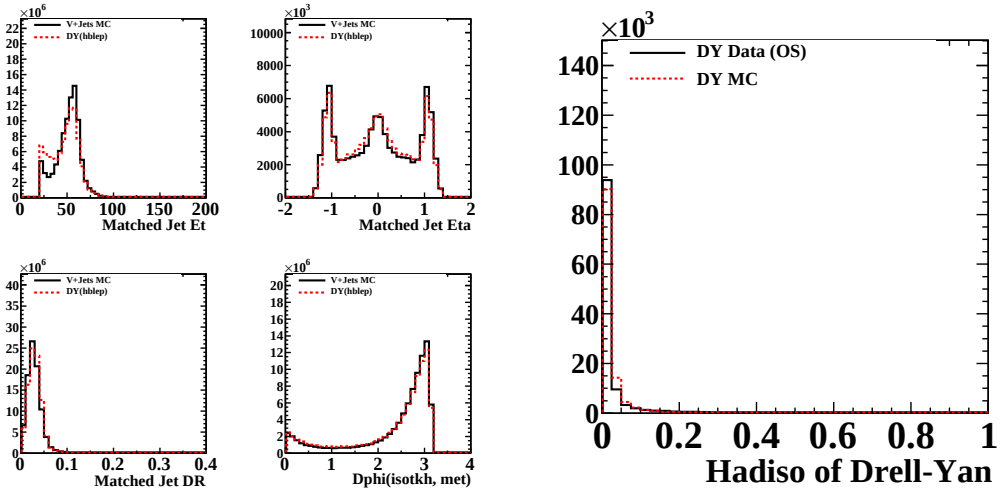

Figure 3: Comparison of matched jet E_T, η, ΔR between the track and matched jet, $\Delta\phi$ between track candidate and$\not\!\!E_T$, and Hadiso, respectively.

4 Background Estimate

We use the same methodology of background estimation in the lepton-triggered analysis, which is commonly referred to as "Method II" [8].

The W+ jets contribution includes jets from b and c quarks, and light-flavor jets mistagged by the b-tagging algorithm. The effect of true W + heavy-flavor production is estimated from a combination of data and simulation. We use both low and high luminosity ALPGEN Monte Carlo samples to calculate the rate of $Wb\bar{b}, Wc\bar{c}$, and Wc production relative to inclusive W + jets production. Then this relative rate is applied to the observed W + jets sample, after non-W and $t\bar{t}$ contributions have been subtracted. Finally, we apply b-tagging efficiencies and b-tagging scale factors to estimate the background after tagging.

Contributions from events with falsely tagged light-flavor jets (mistags) are estimated using the latest version of the mistag matrices [9] for SecVtx, JP, and RomaNN b-tagging algorithms.

The normalization of the diboson, $t\bar{t}$ and single top backgrounds are based on the theoretical cross sections (listed in Table 2). The event acceptance and b-tagging efficiency are derived from MC. The acceptance is corrected in MC events for lepton identification, trigger efficiencies and z vertex cut, and b-tagging scale factors.

The signature of W decay can also be mimicked by non-W multijet events which may contain a high-energy reconstructed lepton and missing transverse energy. These can arise from semileptonic heavy-flavor decay or from false reconstructions. The reconstructed leptons from such events are rarely isolated from the rest of the event, as required by our event selection. We therefore calculate the number of non-W events in our selected sample by extrapolating from non-W control region into the signal region.

Theoretical Cross Sections	
WW	11.66 ± 0.70 pb
WZ	3.46 ± 0.30 pb
ZZ	1.51 ± 0.20 pb
Single Top s-channel	1.05 ± 0.07 pb
Single Top t-channel	2.10 ± 0.19 pb
$Z +$ jets	787.4 ± 85.0 pb
$t\bar{t}$	7.04 ± 0.6 pb

Table 2: Theoretical cross sections and errors for the electroweak and single top backgrounds, along with the theoretical cross section for $t\bar{t}$.

4.1 Non-W (QCD fake) background

Loose Electron We estimate the non-W background in the pretag and tagged samples by fitting the $\not\!\!E_T$ distribution to signal and background templates. The signal template is obtained from the Z+jet, W+LF, top, and electroweak Monte Carlo samples. The non-W distribution is obtained from the loose electron with the likelihood < 0.1. The comparison of $\not\!\!E_T$ distributions with various electron likelihood cuts is shown in Figure 4 that a cut of 0.1 on the likelihood seems provide an ideal non-W sample. We also compared the kinematic of such sample with the standard anti-electron sample that their $\not\!\!E_T$ seems quite similar, but not the electron E_T, as shown in Figure 4.

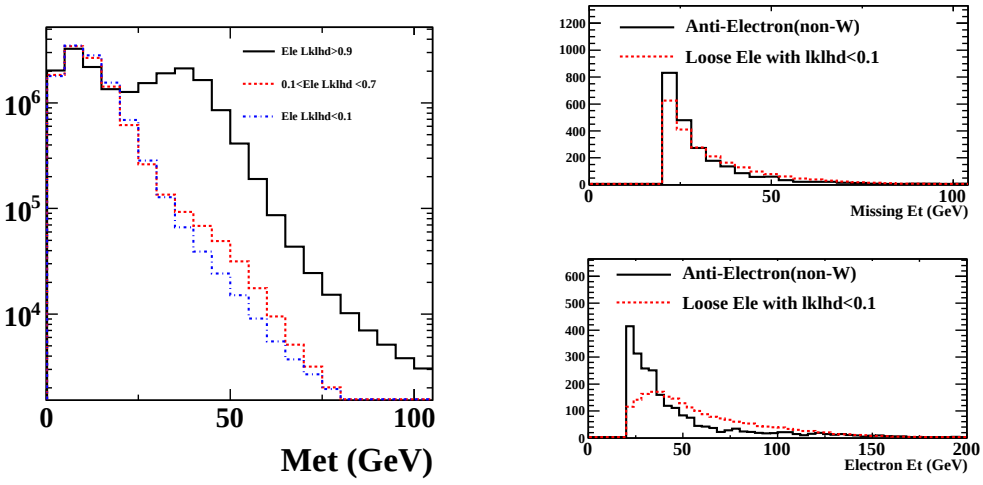

Figure 4: Comparison of $\not\!\!E_T$ distributions with various electron liklihood cuts is on left and comparison to the anti-electron sample is on right.

indicates failed at least two standard electron cuts with additional corrections of loose electron ID efficiency.

Looser Isolated Track We estimate the non-W fraction in the pretag and tagged samples by fitting the data Hadiso distribution to signal and background templates. The MC signal template contains events from Z+jet, W+LF, top, and electroweak backgrounds. The non-W distribution is obtained from the jets containing a loose muon (CMU, CMP, CMUP, BMU) that failed at least two standard muon cuts, but passed the isolated track selection. The same-sign pair provides an alternative sample of fakes from the W+jets. The comparison is shown in Figure 5 that seems agree each other. However, these loose muon events may introduce some bias on the Q*η because of the stub requirement. Figure 6 shows the Q*η distributions from the looser isolated track and the loose muon in the 1jet bin that is used to correct for Q*η of the loose muon in the 2jet bin.

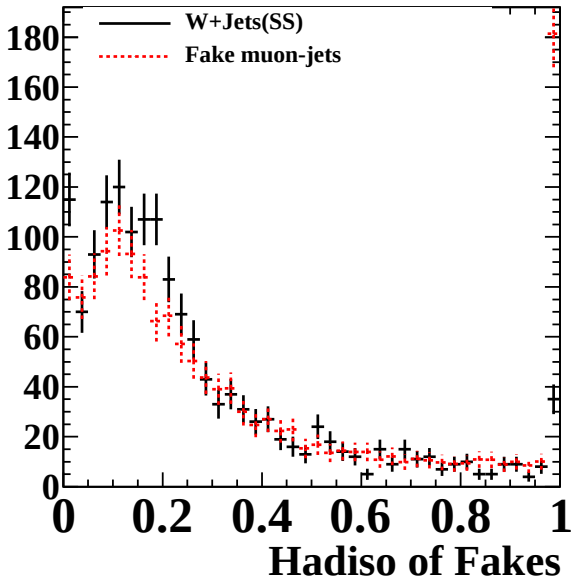

Figure 5: The comparison of Hadiso for various non-W background.

We use the same uncertainty estimates as described in "Method II For You" [8], which was determined by performing fits with an alternative shape, a variety of binnings and fit ranges. The relative uncertainty on the non-W normalization is 40%. Figure 7-8 show the results fitting the$\not\!\!E_T$ and the Hadiso distribution in the pretag and tag regions for the loose electron and the looser isolated track, respectively. The fits in the double tagged region suffers from low statistics. The uncertainty of 40% accomodates the low statistics.

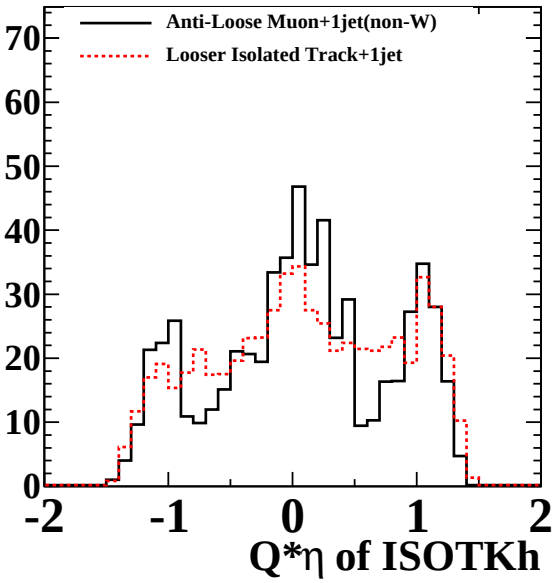

Figure 6: The comparison of Q*η between the looser isolated track and the loose muon non-W in the 1jet bin.

4.2 Background Summary

We have described the contributions of individual background sources to the final background estimate. The summary of the background estimates is shown in Tables 3 - 5 and the number of expected events with observed data as function of jet multiplicity plots are shown in Figures 9 - 11. In general, the number of expected events and the number of observed events are in good agreement.

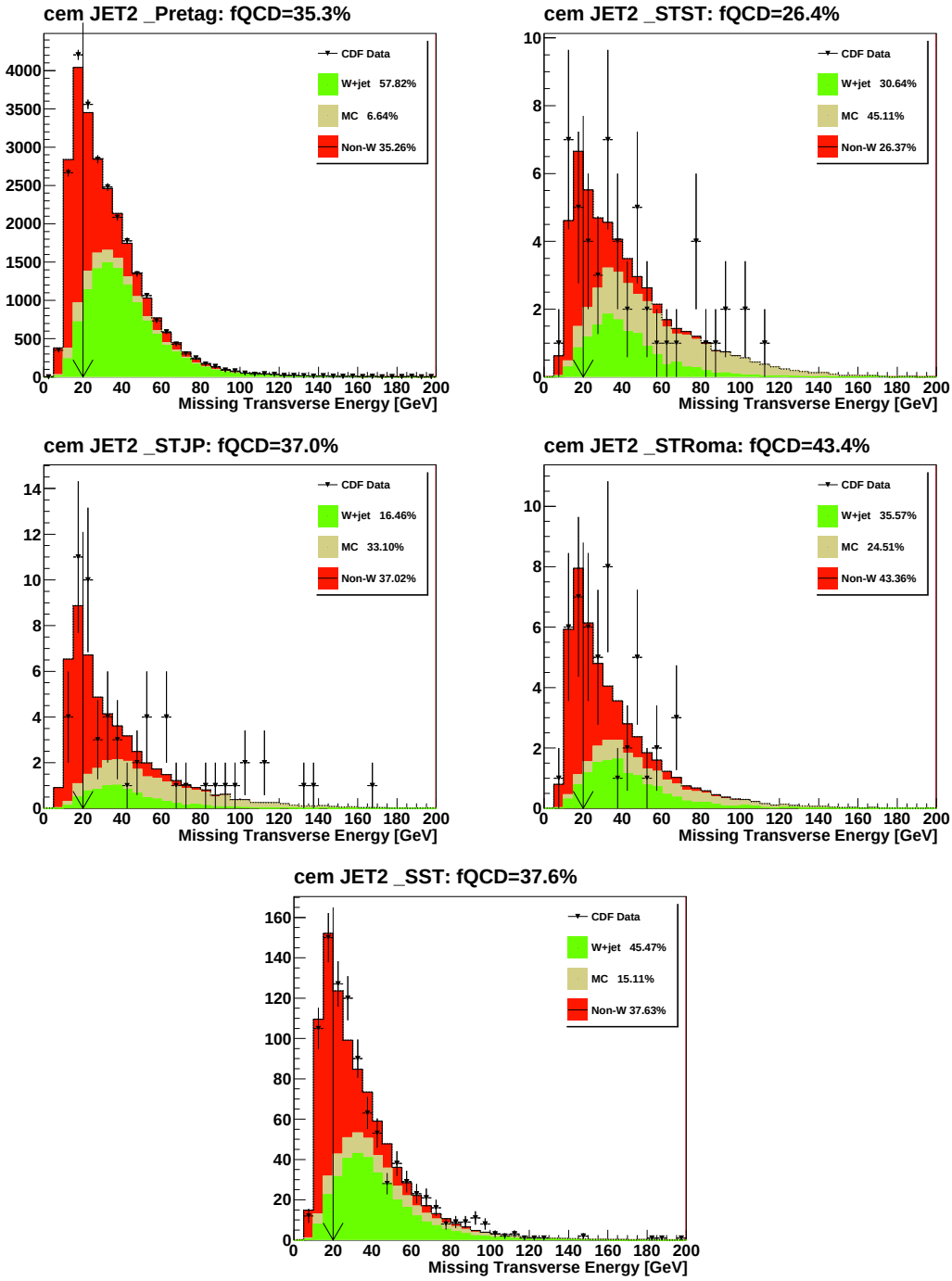

Figure 7: QCD fraction estimate for Pretag and each b-tagging category (STST, STJP, STRoma, SST) in the W + 2 jets events with loose electrons.

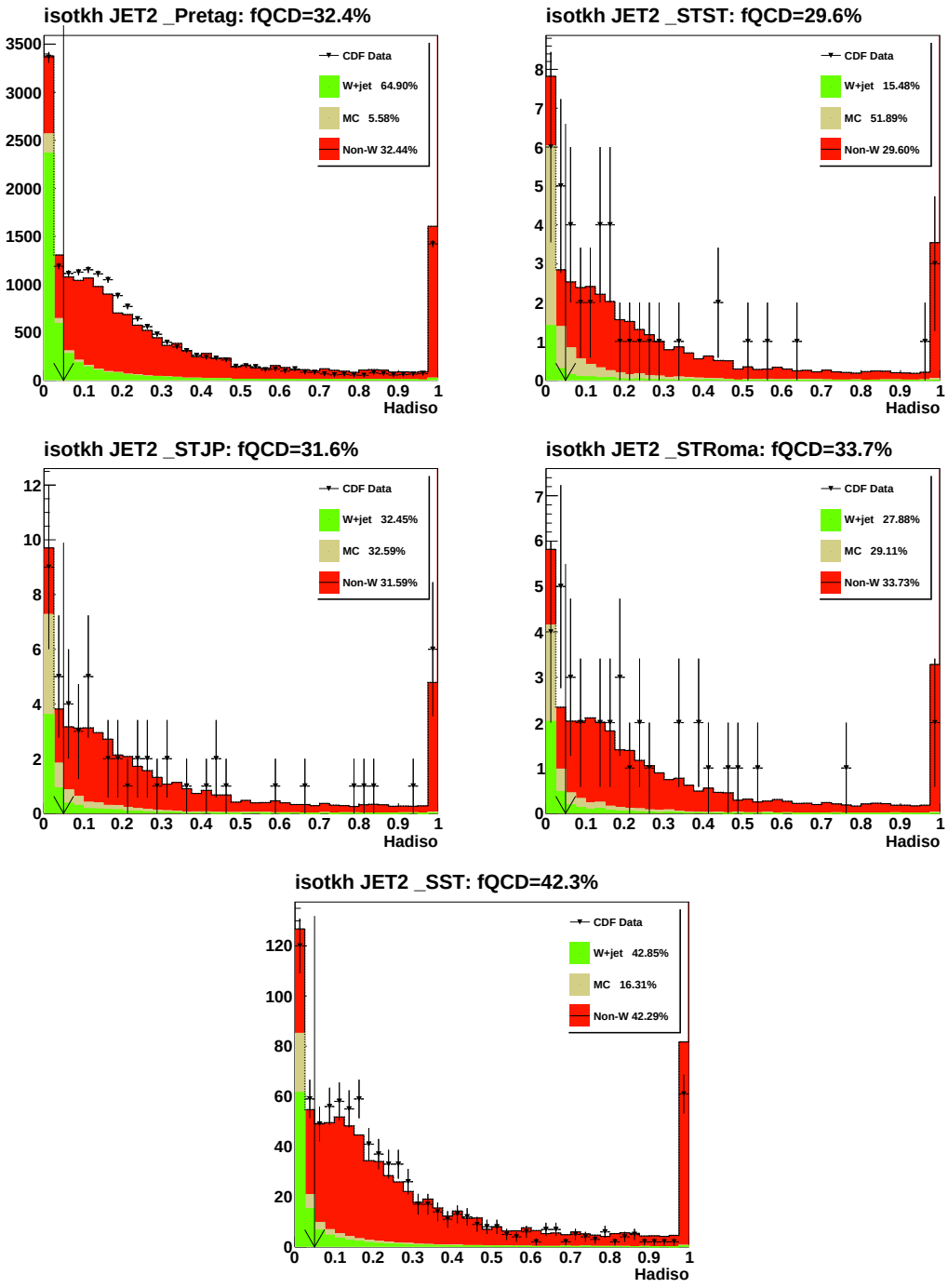

Figure 8: QCD fraction estimate for Pretag and each b-tagging category (STST, STJP, STRoma, SST) in the W + 2 jets events with looser isolated tracks.

Sources	Pretag	STST	STJP	STRoma	SST
Pretag Events	1.83e+04	1.83e+04	1.83e+04	1.83e+04	1.83e+04
W + LF	8.36e+03±2.66e+03	0.83±0.4	1.87±0.86	2.97±1.31	99.8±35.9
W + bb	396±153	18.5±7.88	17.3±6.88	9.44±3.67	86.7±34.1
W + cc	823±318	1.28±0.52	3.18±1.29	2.05±0.81	53.9±21.5
W + cj	979±379	1.52±0.62	3.78±1.53	2.44±0.97	64.2±25.6
t#bart (7.4 pb)	130±11.2	12.7±2.67	9.58±1.19	5.39±0.47	41.6±4.71
Single Top S	27±2.44	3.58±0.76	2.59±0.32	1.43±0.13	8.46±0.92
Single Top T	43.4±4.74	1.08±0.24	0.9±0.14	0.62±0.07	16.3±2.38
WW	335±28.5	0.16±0.03	0.32±0.06	0.27±0.04	16.2±2.47
WZ	52±5.49	0.92±0.2	0.8±0.12	0.43±0.05	4.29±0.59
ZZ	1.98±0.29	0.03±0.01	0.03±0	0.01±0	0.19±0.03
Z + jets	998±87.3	0.66±0.14	0.61±0.11	0.47±0.08	27.4±4.4
Non-W	6.44e+03±2.58e+03	10.8±4.32	16.3±6.51	14.3±5.72	252±101
Total background	1.86e+04±3.78e+03	52.2±10.5	57.3±11.2	39.8±7.67	671±129
WH115	4±0.24	0.53±0.11	0.39±0.04	0.21±0.01	1.24±0.1
Data	1.83e+04	41	44	33	670

Table 3: Background summary table for the loose electron + 2jets in each b-tagging category.

Sources	Pretag	STST	STJP	STRoma	SST
Pretag Events	4.55e+03	4.55e+03	4.55e+03	4.55e+03	4.55e+03
W + LF	2.4e+03±678	0.26±0.12	0.61±0.27	0.89±0.36	27.2±8.98
W + bb	119±44.6	5.15±2.14	4.45±1.71	2.79±1.05	22.5±8.55
W + cc	223±83.4	0.34±0.14	0.94±0.37	0.64±0.25	13.8±5.34
W + cj	214±79.8	0.33±0.13	0.9±0.36	0.62±0.24	13.2±5.1
t#bart (7.4 pb)	63.2±8.11	5.94±1.36	4.77±0.76	2.63±0.34	20.5±3.03
Single Top S	12.2±1.6	1.65±0.38	1.2±0.19	0.66±0.09	3.88±0.56
Single Top T	19.5±2.83	0.55±0.13	0.44±0.08	0.28±0.04	7.3±1.27
WW	134±17.1	0.05±0.01	0.17±0.03	0.12±0.02	6.8±1.22
WZ	21.1±2.99	0.4±0.09	0.28±0.05	0.17±0.02	1.8±0.31
ZZ	0.83±0.14	0.01±0	0.01±0	0.01±0	0.07±0.01
Z + jets	187±24	0.26±0.06	0.28±0.06	0.22±0.04	6.34±1.19
Non-W	1.48e+03±591	3.26±1.3	4.42±1.77	3.04±1.21	75.7±30.3
Total background	4.87e+03±919	18.2±3.34	18.5±3.07	12.1±1.96	199±36.4
WH115	1.58±0.18	0.21±0.05	0.16±0.02	0.08±0.01	0.51±0.06
Data	4.55e+03	11	14	9	179

Table 4: Background summary table for the looser isolated track + 2jets in each b-tagging category.

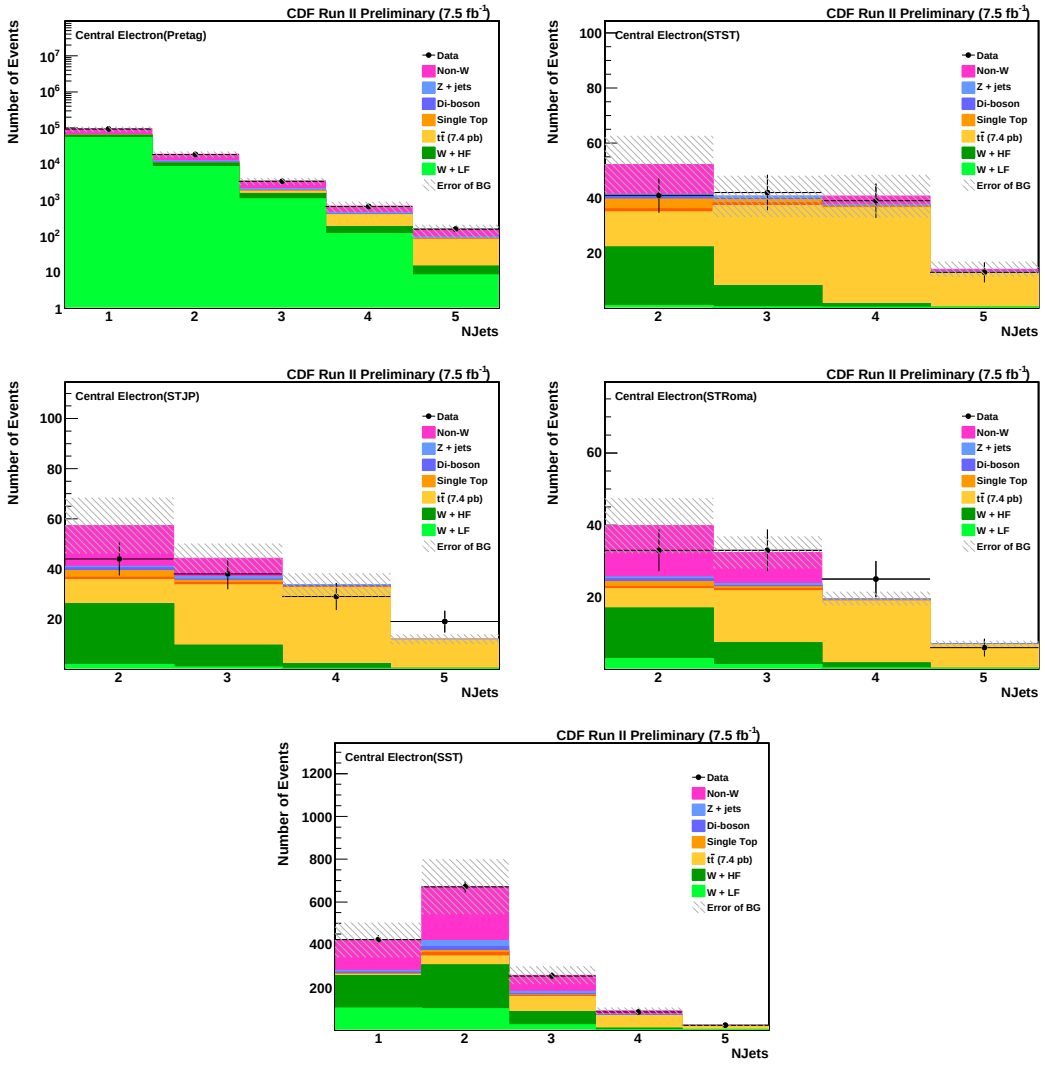

Figure 9: Number of expected and observed events as a function of jet multiplicity in the loose electron channel for each b-tagging category.

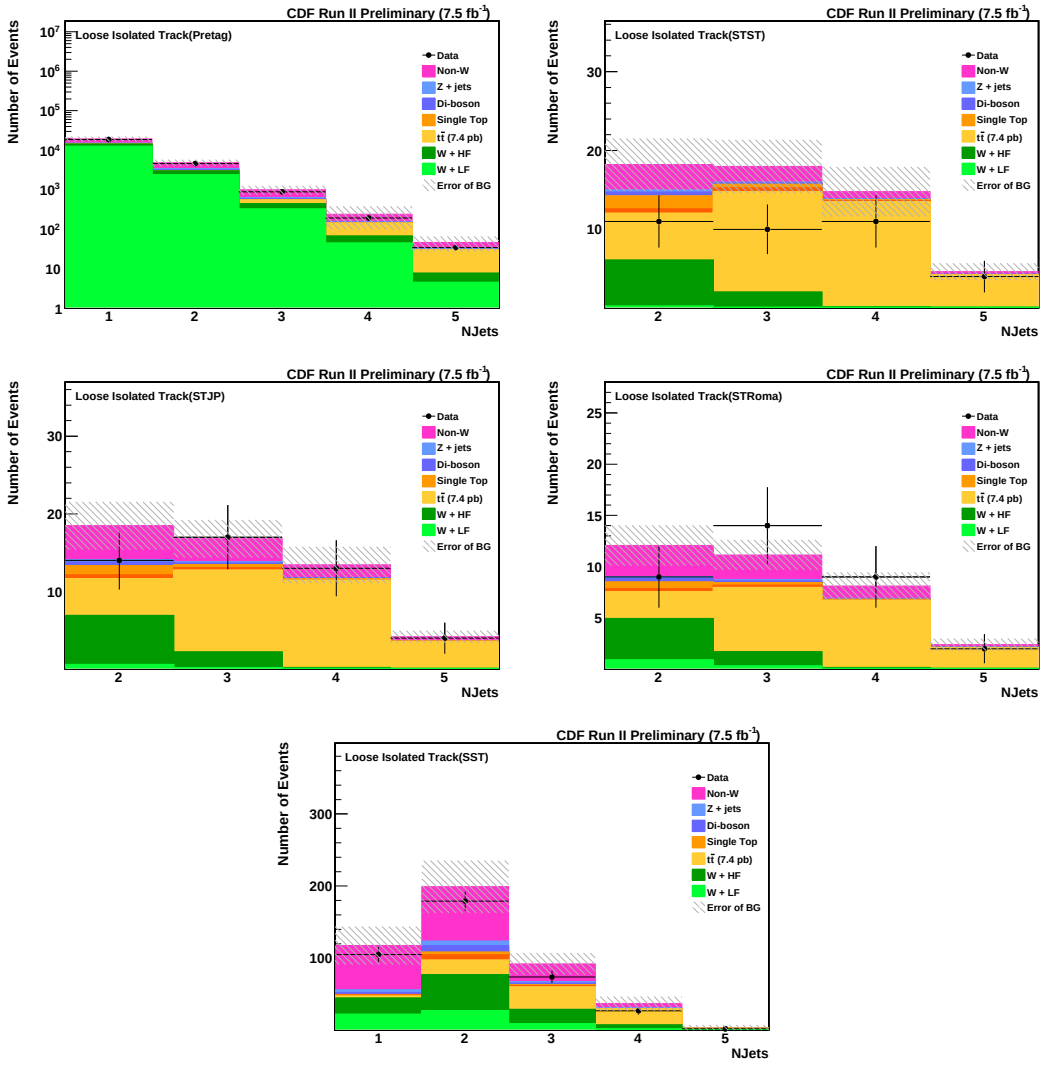

Figure 10: Number of expected and observed events as a function of jet multiplicity in the looser isolated track channel for each b-tagging category.

Sources	Pretag	STST	STJP	STRoma	SST
Pretag Events	2.28e+04	2.28e+04	2.28e+04	2.28e+04	2.28e+04
W + LF	1.08e+04±2.74e+03	1.09±0.47	2.48±1.03	3.86±1.53	127±39
W + bb	515±184	23.7±9.48	21.8±8.08	12.2±4.41	109±40
W + cc	1.05e+03±376	1.62±0.62	4.12±1.56	2.69±0.99	67.8±25.3
W + cj	1.19e+03±433	1.85±0.72	4.68±1.79	3.06±1.13	77.4±29.2
t#bart (7.4 pb)	193±17.8	18.7±3.95	14.4±1.85	8.03±0.75	62.1±7.29
Single Top S	39.2±3.73	5.23±1.12	3.79±0.48	2.09±0.2	12.3±1.38
Single Top T	63±7.12	1.63±0.36	1.34±0.2	0.9±0.11	23.6±3.52
WW	470±41.9	0.21±0.04	0.48±0.09	0.38±0.06	23±3.56
WZ	73.1±7.96	1.32±0.29	1.08±0.16	0.59±0.06	6.09±0.86
ZZ	2.8±0.42	0.04±0.01	0.04±0.01	0.02±0	0.26±0.05
Z + jets	1.18e+03±105	0.92±0.2	0.89±0.17	0.69±0.12	33.8±5.46
Non-W	7.91e+03±3.17e+03	14.1±5.63	20.7±8.28	17.3±6.94	328±131
Total background	2.34e+04±4.29e+03	70.3±13.3	75.7±13.8	51.9±9.39	870±162
WH115	5.58±0.37	0.74±0.15	0.55±0.06	0.3±0.02	1.74±0.15
Data	2.28e+04	52	58	42	849

Table 5: Combined Background summary table for the loose leptons + 2jets in each *b*-tagging category.

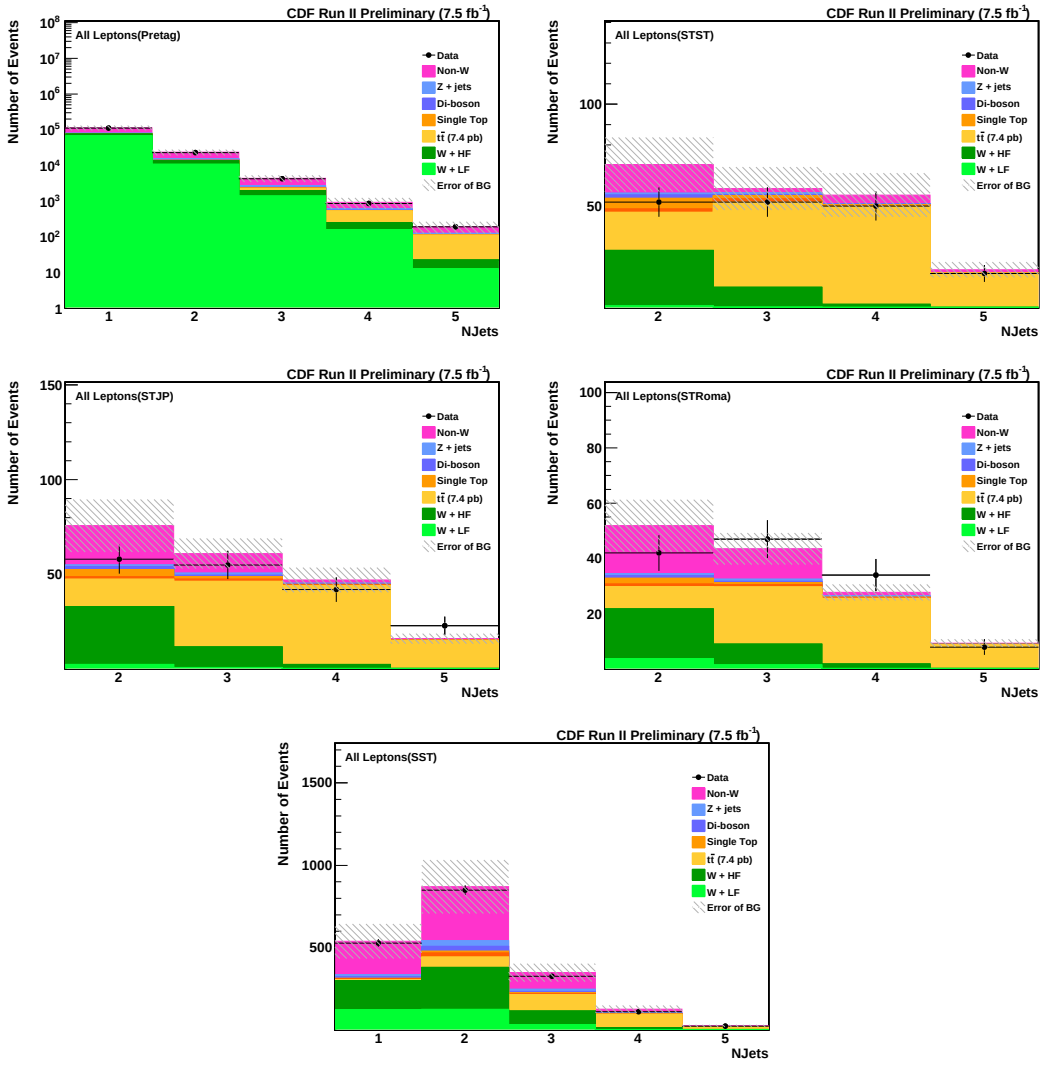

Figure 11: Combined number of expected and observed events as a function of jet multiplicity for each b-tagging category.

$M(H)$	$\sigma(p\bar{p} \to W^{\pm}H)$	Br$(H \to b\bar{b})$
100	0.298 pb	0.812
105	0.253 pb	0.796
110	0.216 pb	0.770
115	0.186 pb	0.732
120	0.160 pb	0.679
125	0.138 pb	0.610
130	0.119 pb	0.527
135	0.104 pb	0.436
140	0.090 pb	0.344
145	0.079 pb	0.256
150	0.069 pb	0.176

Table 6: Theoretical cross section and branching ratio to $b\bar{b}$ for a variety of Higgs masses.

b-tagging category	IsoTrk Reco	Trigger	ISR/FSR/PDF	JES	b-tagging	Total
One tag	8.85%	2%	8.4%	4.7%	4.3%	13.9%
ST + ST	8.85%	2%	7.1%	1.7%	8.6%	14.5%
ST + JP	8.85%	2%	6.4%	2.4%	8.1%	14.0%
ST + RomaNN	8.85%	2%	19.5%	1.9%	13.6%	25.5%

Table 7: Systematic uncertainties for IsoTrks.

5 Signal Acceptance

Samples of Pythia $WH \to l\nu b\bar{b}$ Monte Carlo with Higgs boson masses between 100 GeV and 150 GeV are used to estimate $\epsilon^{MC}_{WH \to l\nu b\bar{b}}$. The MC samples were generated with beam conditions which approximate real data periods, for run periods 0-18.

Table 6 shows the NNLO WH production cross section and the branching ratio of $H \to b\bar{b}$. The cross sections and the branching ratios in table 6 are multiplied with the integrated luminosity, 7.6 fb^{-1}, and the overall event detection efficiencies to produce the number of expected WH events as shown in Table 5. According to WH115 signal Monte Carlo, the gain of the WH acceptance is about 40% of the central electron channel.

5.1 Other Systematic Uncertainties on Acceptance

The systematic uncertainties on the acceptance include uncertainties from the jet energy scale, initial and final state radiation contribution, and the b-tagging scale factor, which are very similar to the uncertainty estimates as described in the standard isolated track analysis [1]. Total systematic uncertainties are listed in Table 7.

6 Kinematic Distributions

The kinematic distribution for all discriminant input variables and NN output distributions have been thoroughly examined to establish proper modeling using pretag sample, see Figures 12 - 16 for the loose electron and Figure 17 - 21 for the looser isolated track lepton. The data and MC background estimates are in good agreement. The same NN inputs and output distributions after b-tagging can be found in Appendix:

- Figure 28 - 32 for STST tags;
- Figure 33 - 37 for STJP tags;
- Figure 38 - 42 for STRoma tags;
- Figure 43 - 47 for SST tags.

We will sum up the two type of loose leptons together after b-tagging to gain some statistics.

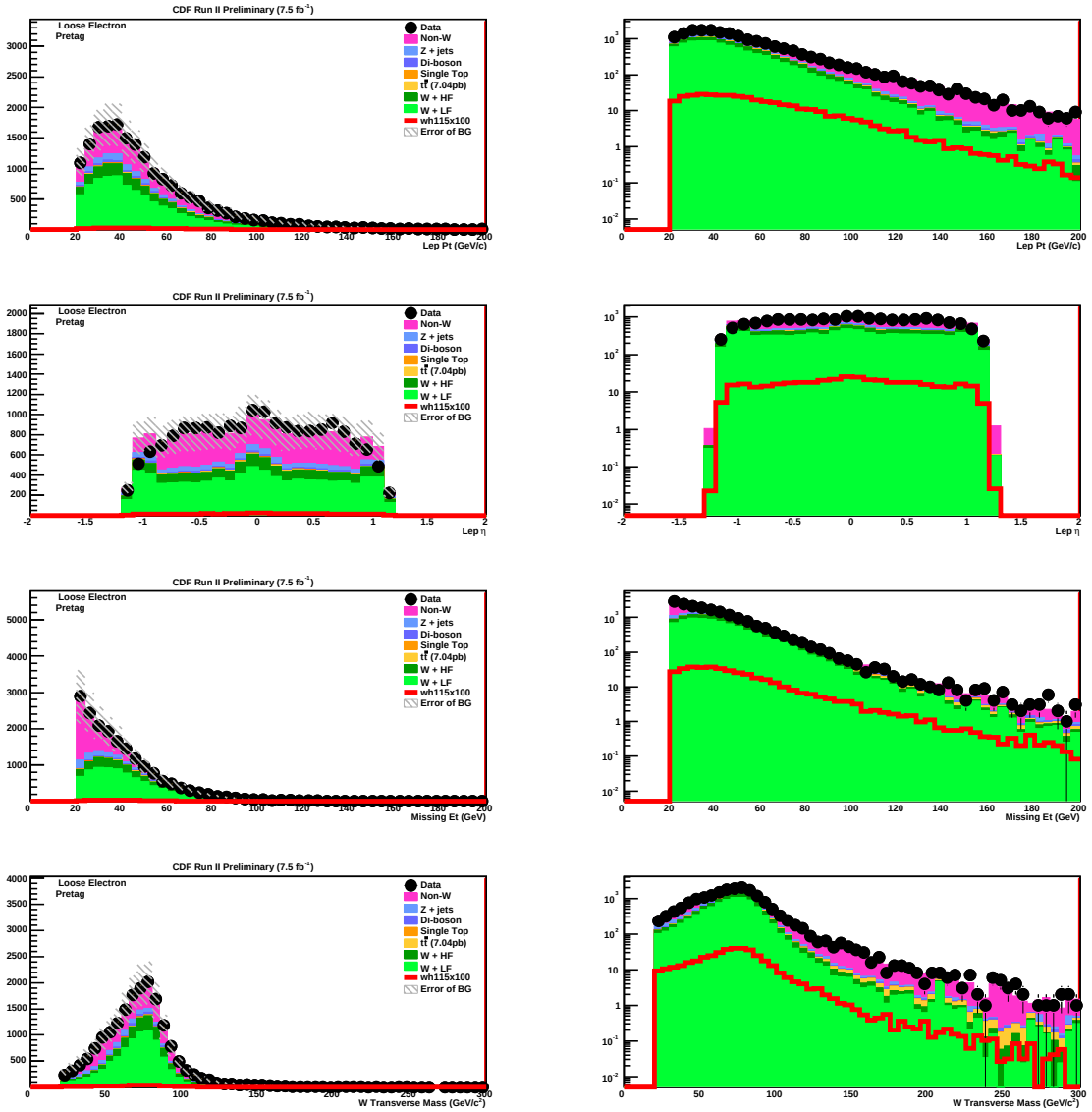

Figure 12: Pretag kinematic distributions for loose electron: p_T, η,$\not\!\!E_T$, and W transverse mass.

7 Shape Systematics

Since the entire histogroms of the BNN output in the selected signal region are used to extract the final result, the shape uncertainties affect the final sensitivity of this analysis.

We estimate Jet Energy Scale (JES) shape uncertainty by shifting the JES with $\pm$ 1 sigma from the nominal value. Figure 22-24 shows the comparison between nominal and $\pm$ 1 sigma shifted BNN templates for the signal and some main backgrounds, such

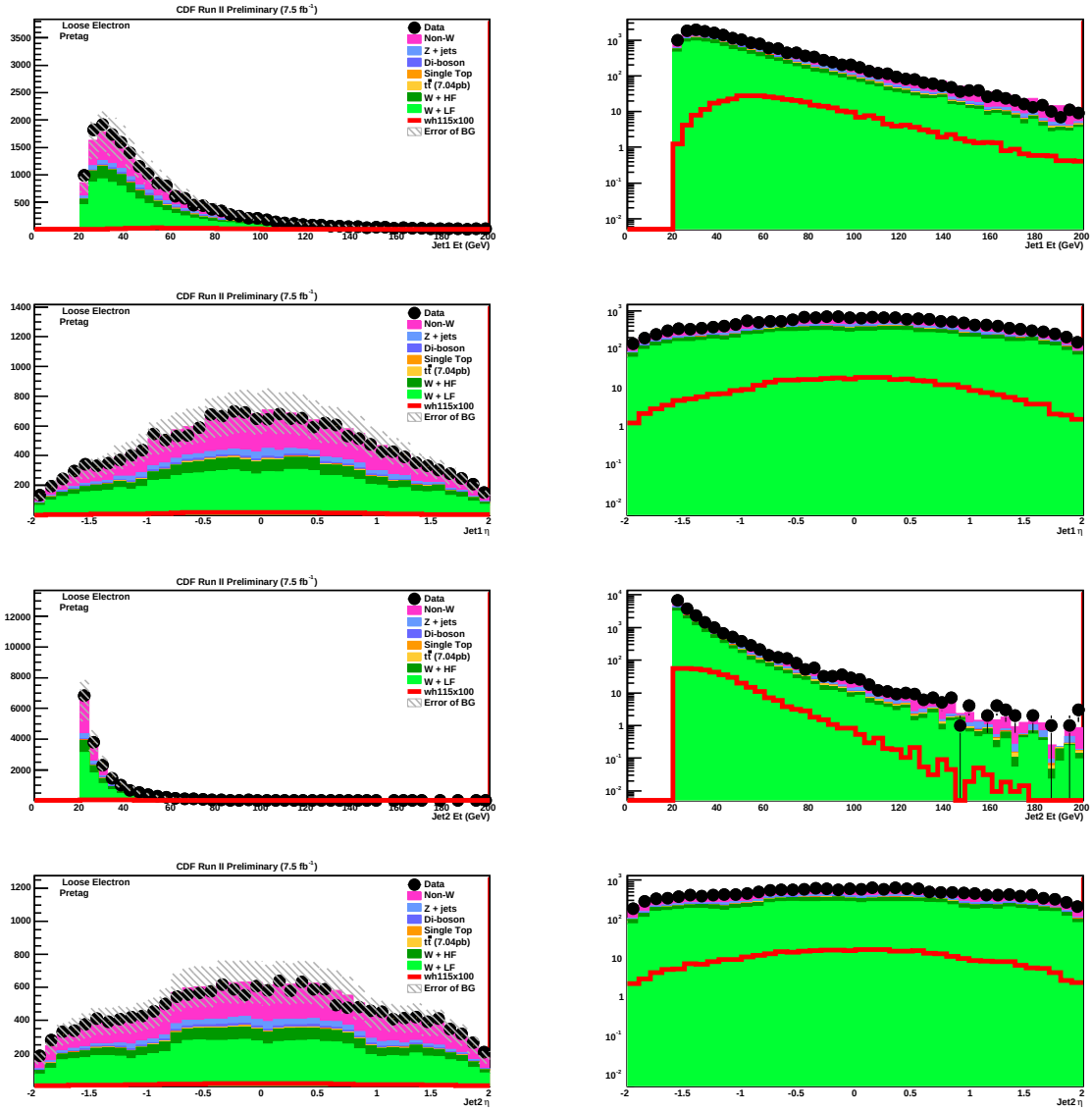

Figure 13: Pretag kinematic distributions for loose electron: first jet E_T, η and second jet E_T, η.

as $W + b\bar{b}$ and $t\bar{t}$, respectively. To extract the limit, we do include the JES shape uncertainty for the signal and all the backgrounds (W+jets ($W + b\bar{b}$, $W + c\bar{c}$, Mistag), $t\bar{t}$, single top (s-channel, t-channel), dibosons (WW, WZ, ZZ), and Z+jets).

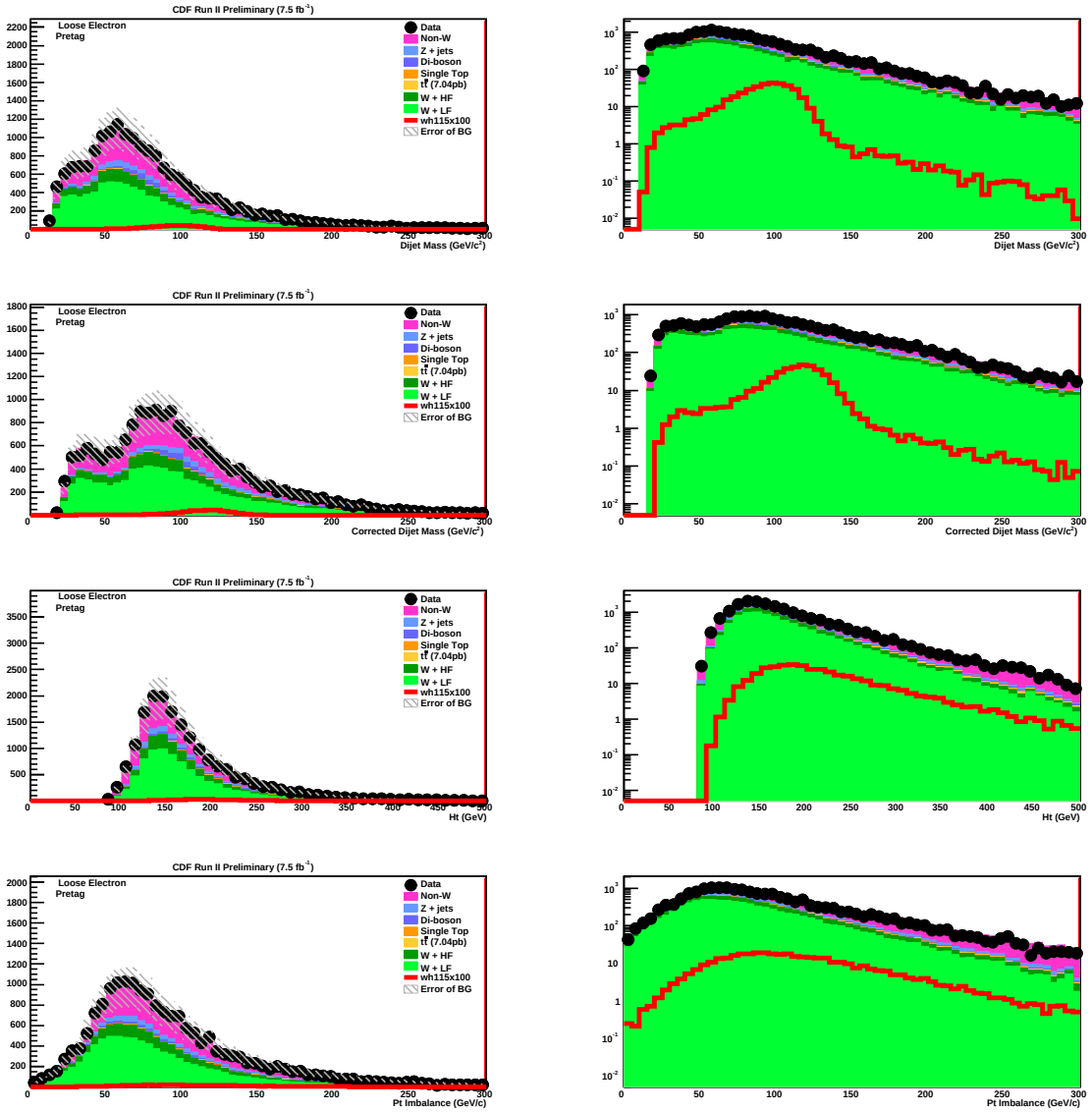

Figure 14: Pretag kinematic distributions for loose electron: dijet mass before and after bjet energy correction, H_T, and P_T imbalance.

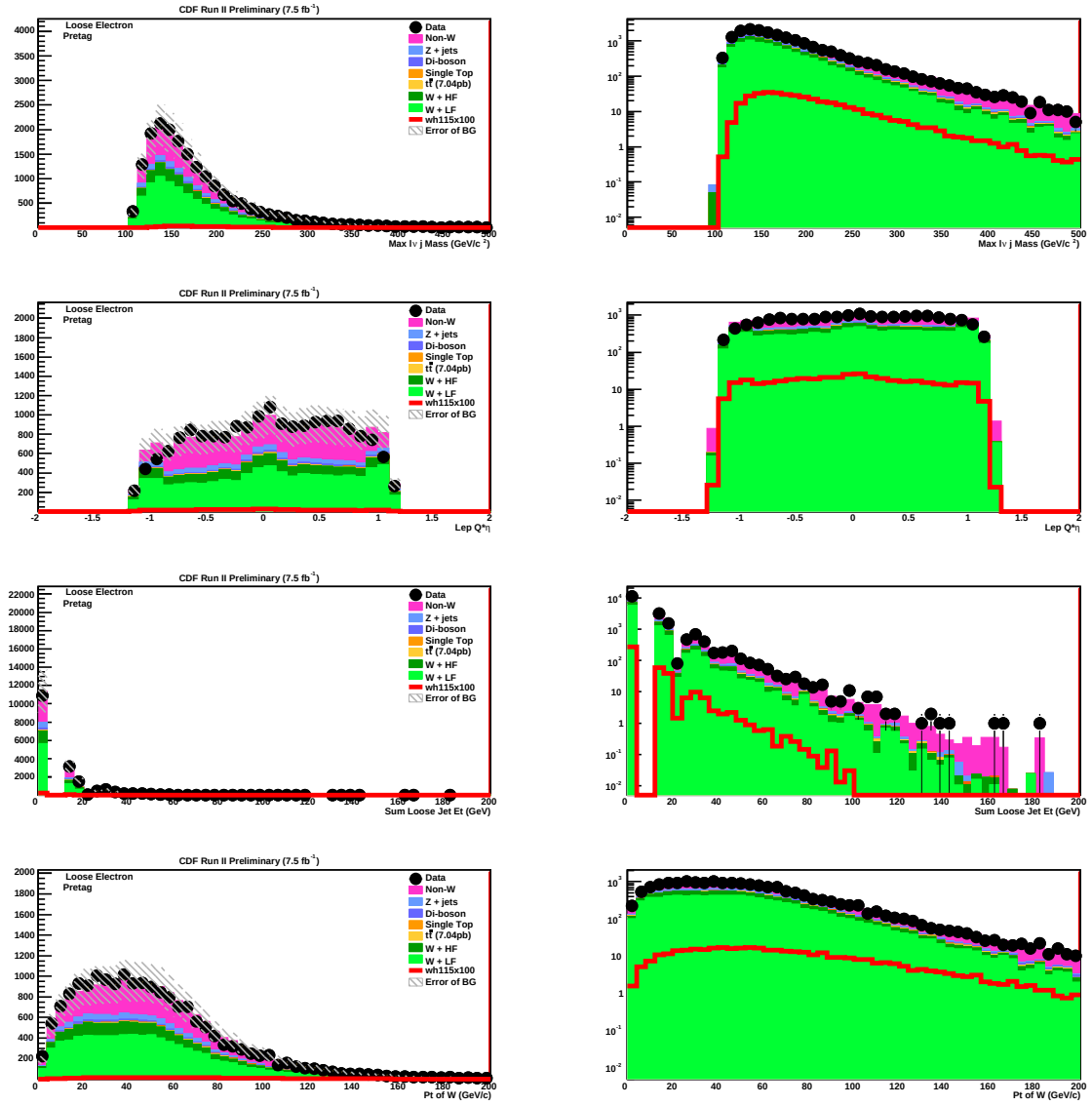

Figure 15: Pretag kinematic distributions for loose electron: maximum of lvj mass, $\eta \times Q$, sum loose jet E_T, and P_T of W candidate.

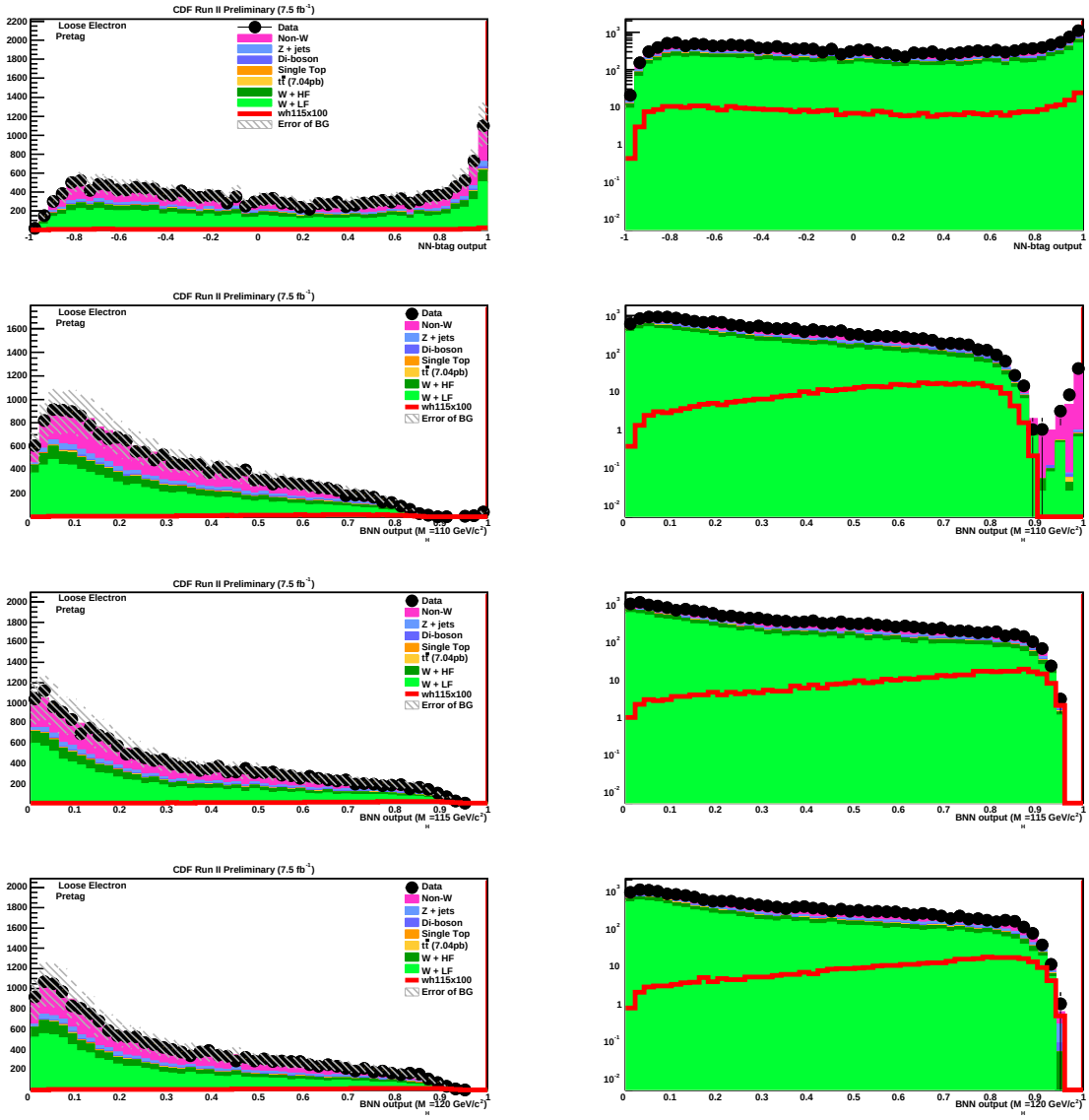

Figure 16: Pretag kinematic distributions for loose electron: kitnn and Bnn output corresponds to m_H =110, 115, 120 GeV/c^2 respectively.

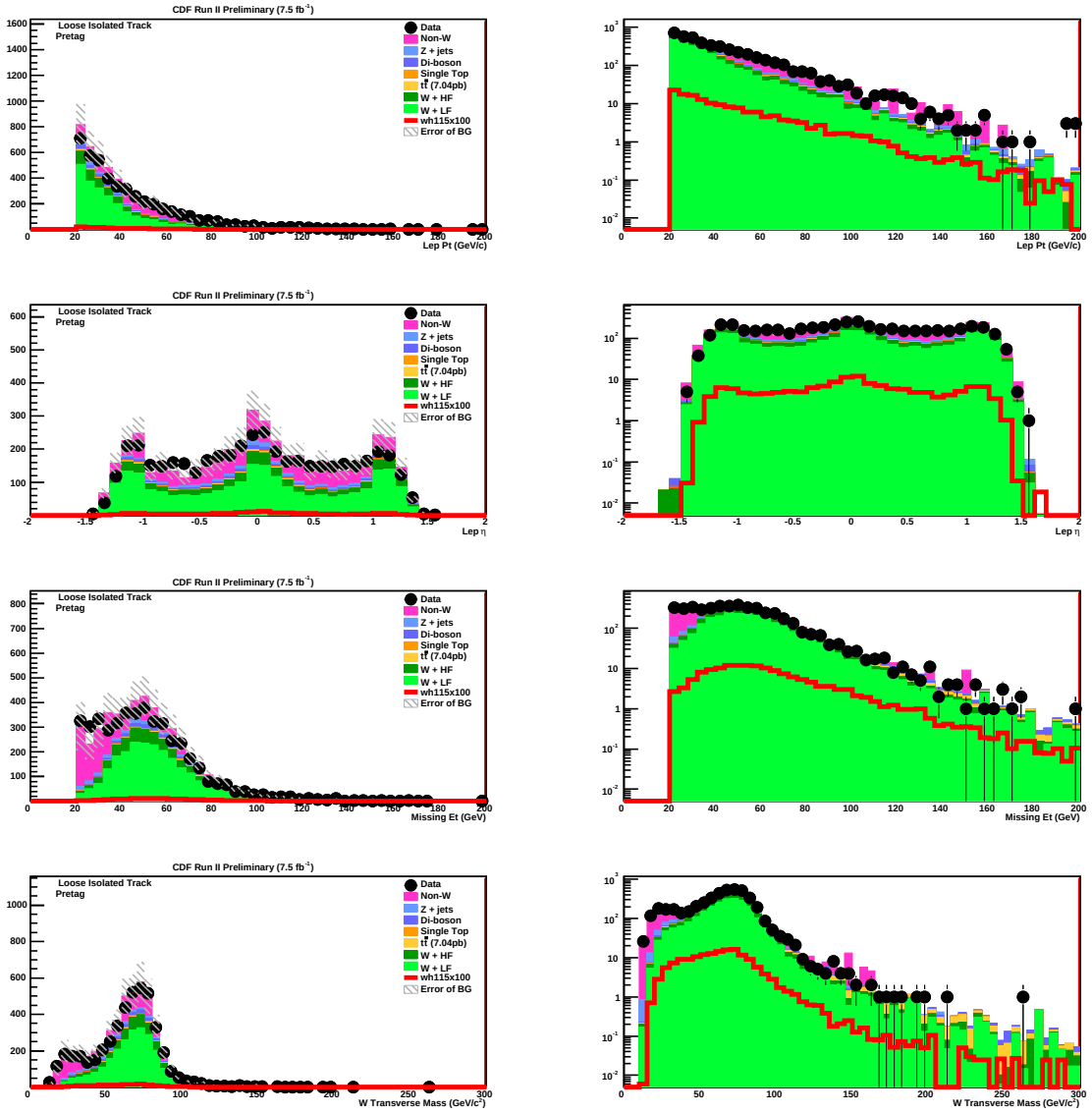

Figure 17: Pretag kinematic distributions for looser isolated track p_T, η, $\not\!\!E_T$, and W transverse mass.

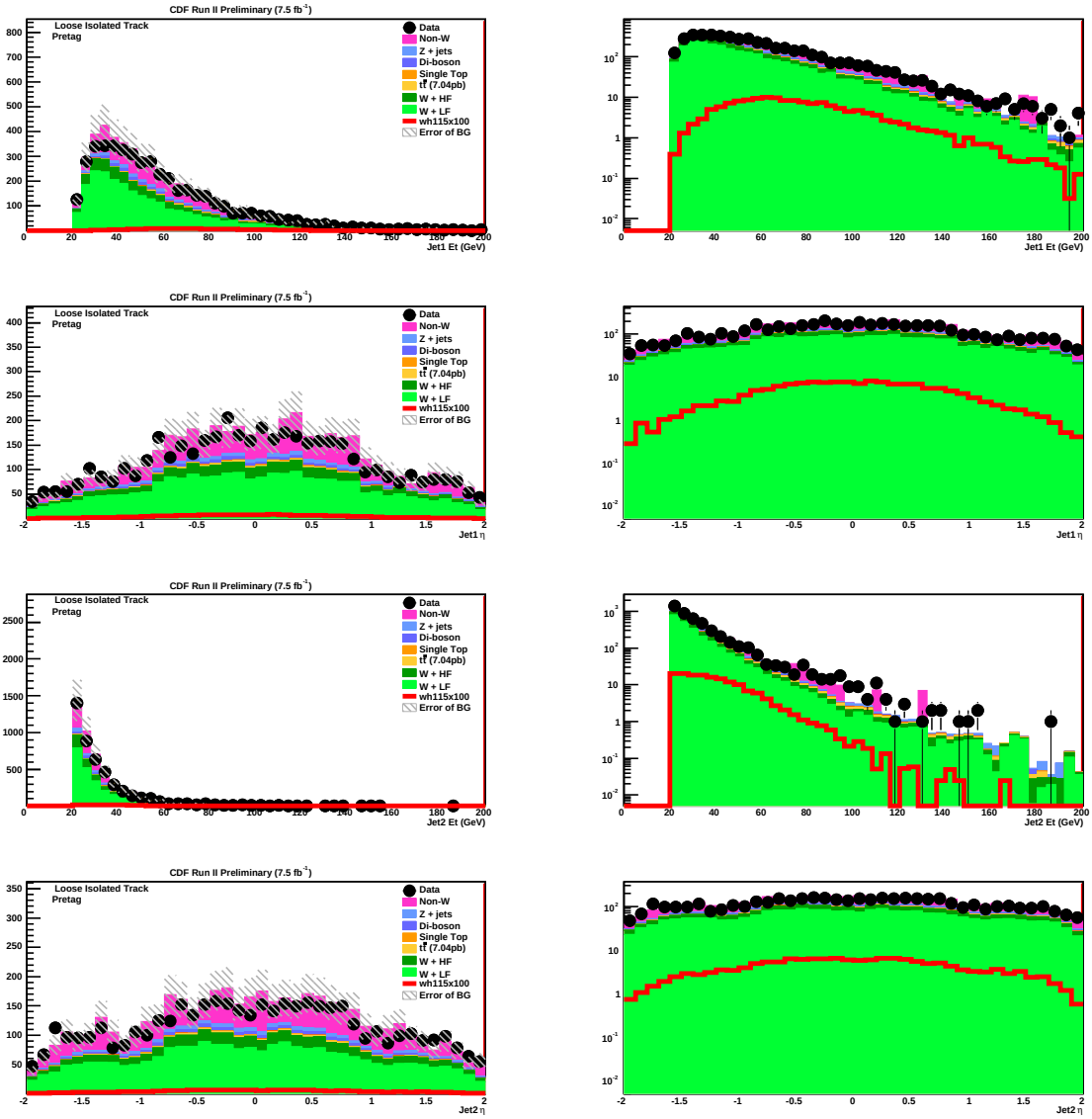

Figure 18: Pretag kinematic distributions for looser isolated track: first jet E_T, η and second jet E_T, η.

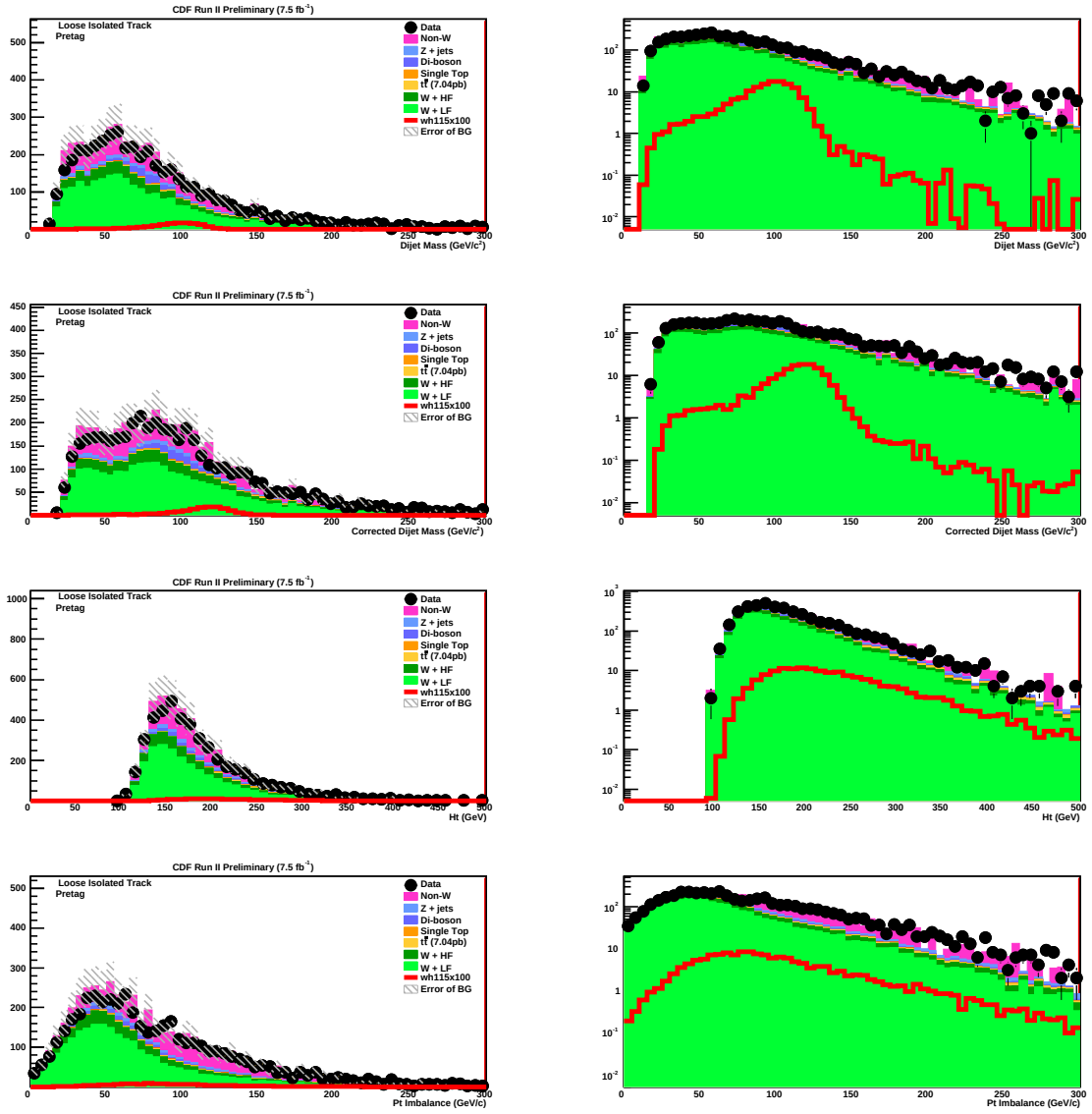

Figure 19: Pretag kinematic distributions for looser isolated track: dijet mass before and after bjet energy correction, H_T, and P_T imbalance.

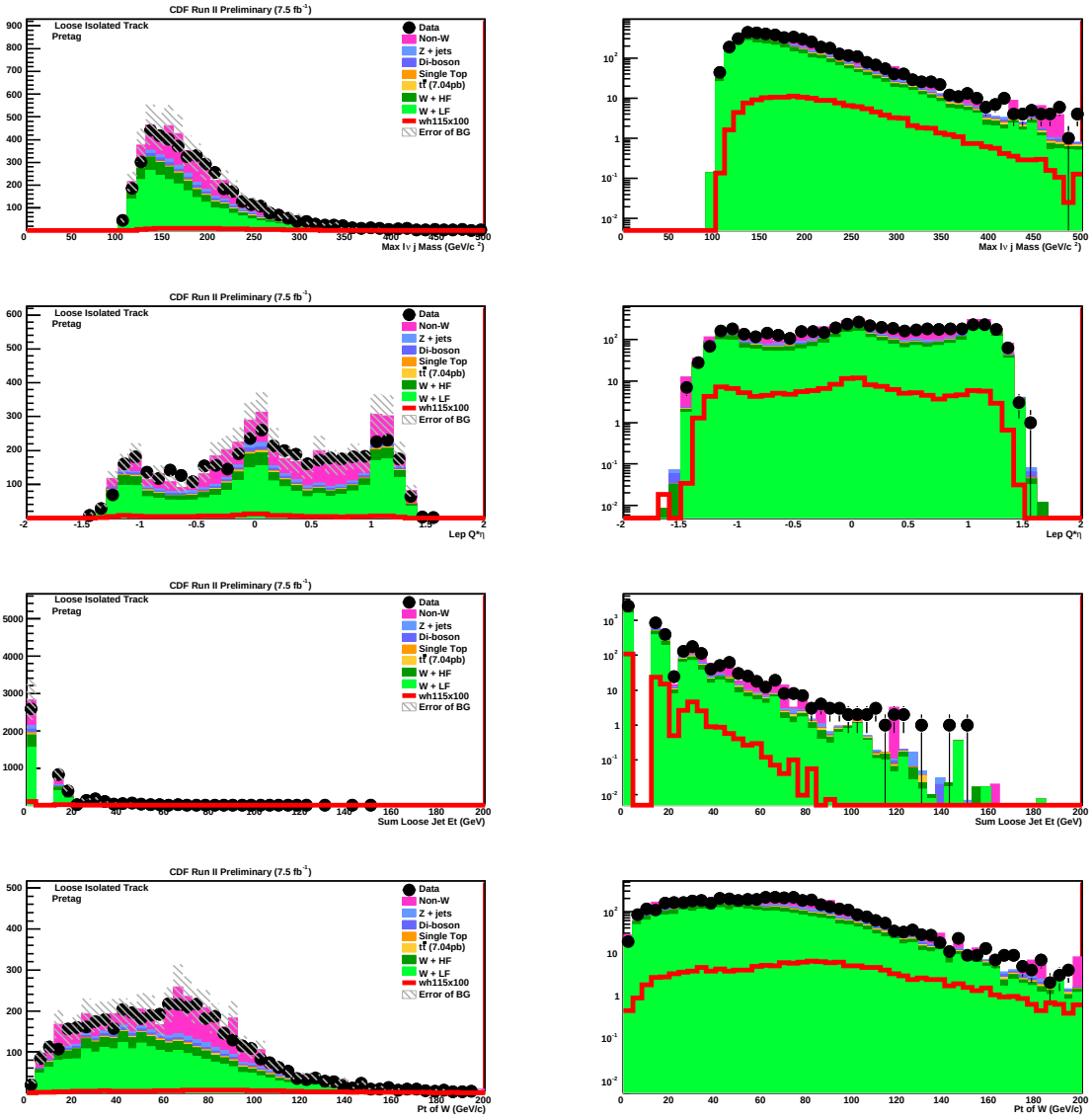

Figure 20: Pretag kinematic distributions for looser isolated track: maximum of lvj mass, $\eta \times Q$, sum loose jet E_T, and P_T of W candidate.

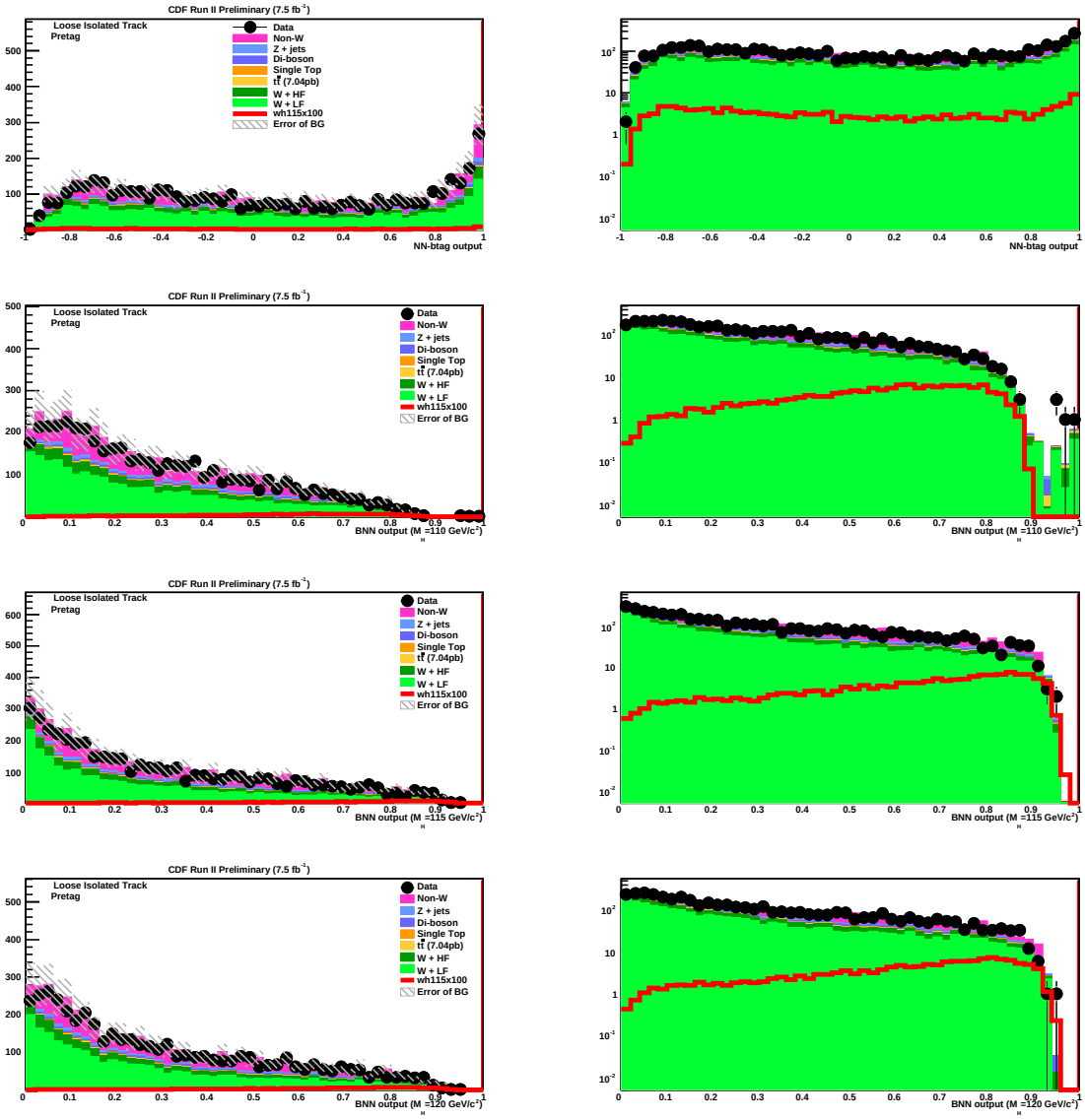

Figure 21: Pretag kinematic distributions for looser isolated track: kitnn and Bnn output corresponds to m_H =110, 115, 120 GeV/c^2 respectively.

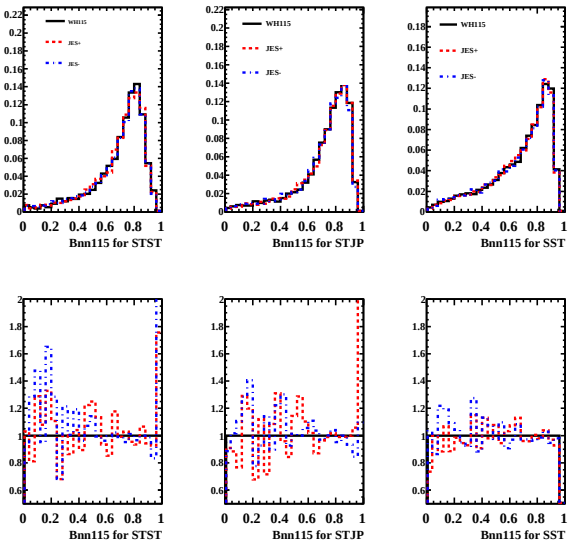

Figure 22: BNN output shape for default and ±1 sigma JES for WH signal (m_H = 115 GeV/c^2). From left to right, tight double(ST+ST), loose double(ST+JP and ST+RomaNN), and single tag(SST), respectively.

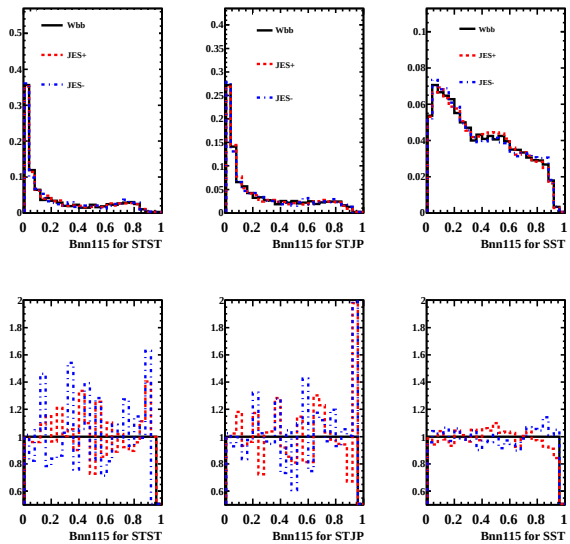

Figure 23: BNN output shape for default and ±1 sigma JES for $Wb\bar{b}$ (m_H = 115 GeV/c^2). From left to right, tight double(ST+ST), loose double(ST+JP and ST+RomaNN), and single tag(SST), respectively.

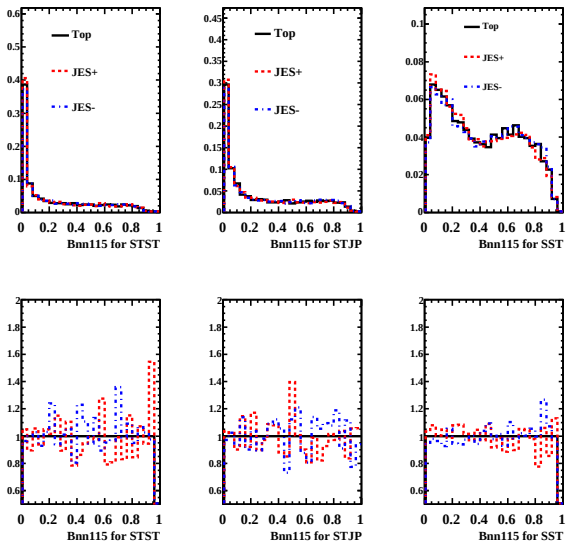

Figure 24: BNN output shape for default and ±1 sigma JES for $t\bar{t}$ ($m_H = 115$ GeV/c^2). From left to right, tight double(ST+ST), loose double(ST+JP and ST+RomaNN), and single tag(SST), respectively.

8 Results

Since there is no significant excess of events in the data compared to the background expectation, we fit the NN output distributions shown in Figure 25 and extract 95% C.L. upper limits for the four tag categories (1-ST, ST+ST, ST+JP and ST+RomaNN) using pseudo-experiments based on the background expectations.

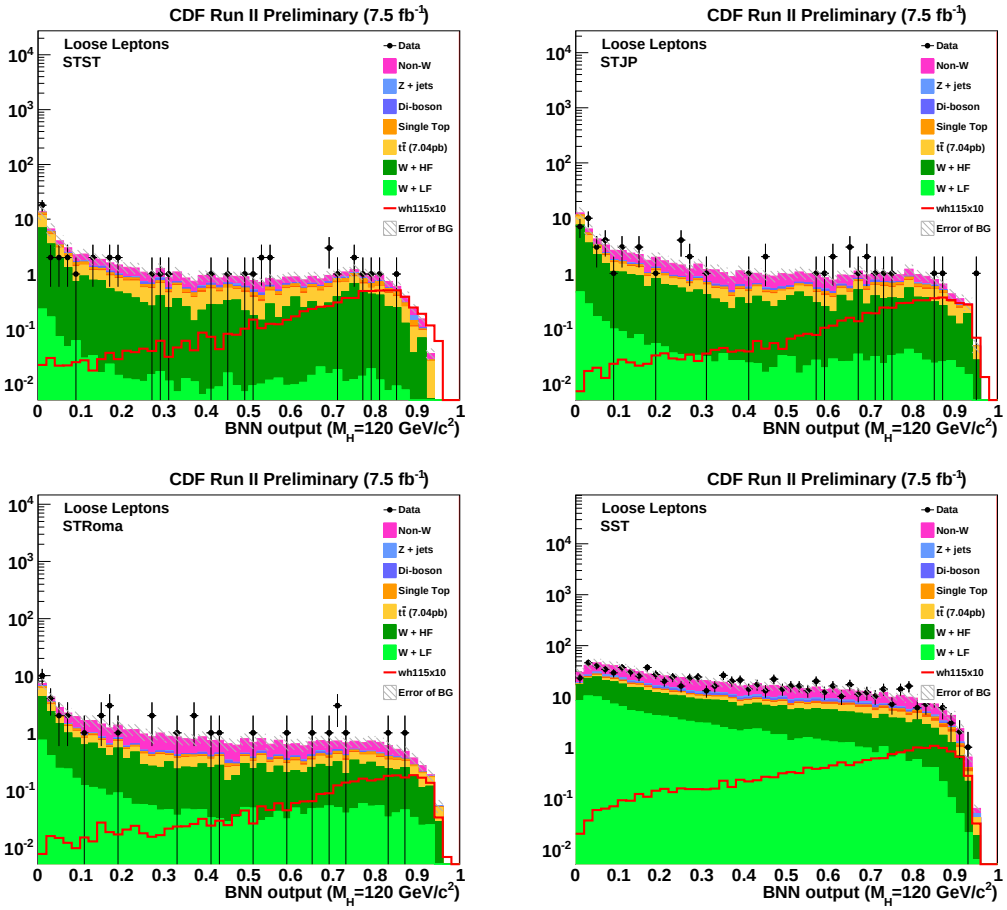

Figure 25: BNN data output in four b-tagging categories (STST, STJP, STRoma, SST) along with background expectations for the Higgs mass hypothesis at $m_H = 120$ GeV/c^2.

The following systematic uncertainties, up to the pretag acceptance, are treated as 100% correlated:

1. luminosity uncertainty
2. uncertainty on the SecVtx b-tag scale factor
3. Jet probability scale factor

CDF Run II Preliminary 7.5 fb^{-1} Limits for Combined Lepton and Tag Categories		
M(H)	Observed Limit	Expected Limit
100	5.1	6.3
105	7.0	7.0
110	8.4	8.1
115	7.9	9.3
120	11.2	11.2
125	14.0	13.3
130	21.1	17.2
135	28.0	23.6
140	48.2	32.3
145	59.3	47.3
150	97.9	77.3

Table 8: Expected and observed limits as a function of Higgs mass for combining the combined all b-tag categories.

4. RomaNN scale factor.

Table 8 details the expected and observed limits at the various Higgs mass points for the combined search across lepton types and tag categories. Figure 26 shows the observed limits and the expected limits with 1σ and 2σ pseudo experiment bands. When combining with the existing WH channels, the WH sensitivity is improved an average of 5.6% for $100 \leq m_H \leq 150$ GeV/c^2, as shown in Figure 27.

8.1 Overlap with Other Channels

In order to quantify the overlap contributions between channels, we have exchanged the event list of WH115 and ZH120 Monte Carlo Signal samples that have been selected by this analysis and $ZH \rightarrow ee b\bar{b}, \mu^+\mu^- b\bar{b}, \not\!\!E_T b\bar{b}$ and found the overlap between channels are small up to 1% so that we can include all for the combination.

9 Conclusions

We present a new selection of W events to be used in the $WH \rightarrow l\nu b\bar{b}$ analysis. The new events are selected by requiring a high P_T track with significant deposits of energy in the calorimeter that are primary from the decay of $W \rightarrow e\nu$ or $\tau\nu$ where the electron failed the standard electron selection or the τ decays into a single charged hadron (one-prong). We find that for the dataset corresponding to integrated luminosity of 7.5 fb^{-1}, the data agree with the SM background predictions within the systematic

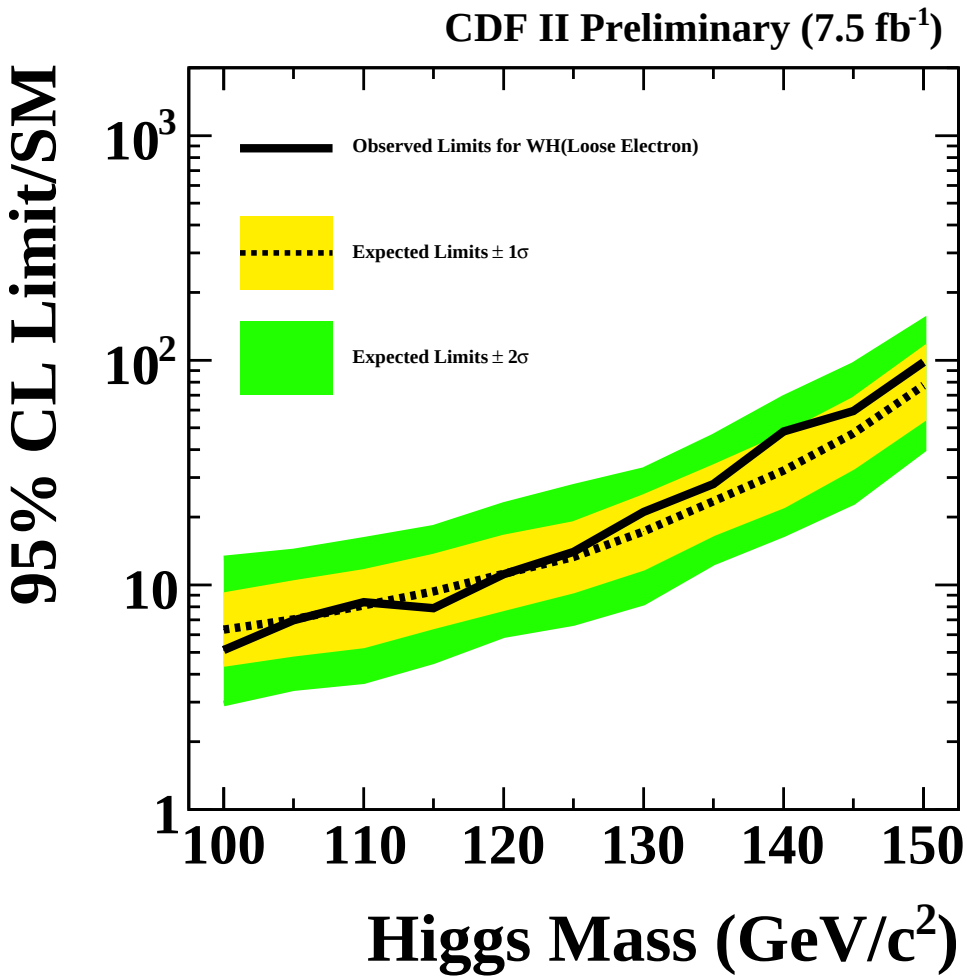

Figure 26: Expected and observed limts for combining all b-tag categories.

uncertainties. We therefore set upper limits on the Higgs production cross section times the $b\bar{b}$ branching ratio. We find $\sigma(p\bar{p} \to W^{\pm}H) \times \mathrm{Br}(H \to b\bar{b})$ with an observed limit 7.9 $\times$ SM prediction (9.3 expected) for $m_h = 115$ GeV/c^2 at 95% confidence level. When combining with the existing WH channels, the WH sensitivity is improved an average of 5.6% for $100 \leq m_h \leq 150$ GeV/c^2.

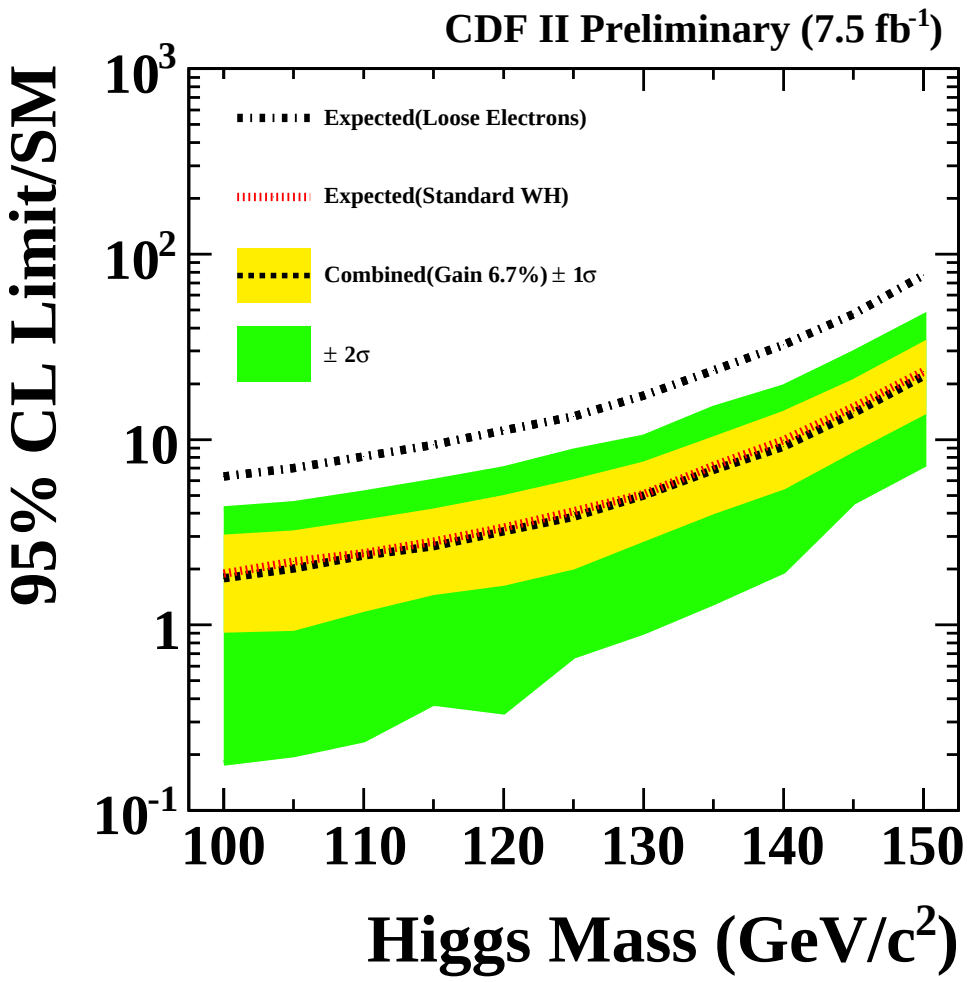

Figure 27: Comparison of the individual and combined expected limts for the WH channel.

References

[1] A. Buzatu *et al.*, "Search for the Standard Model Higgs Boson Production in Association with a W Boson using 7.6 fb^{-1}, " CDF Note 10571;
Y. Nagai *et al.*, "Search for Higgs Boson Production in Association with a W Boson using $\int \mathcal{L}dt = 4.8$ fb^{-1}," CDF Note 10145.

[2] D. Benjamin *et al.*, "Updated Search for $H \to W^+W^-$ Production using 4.8 fb^{-1}," CDF Note 9863.

[3] Y. Nagai *et al.*,"Improving WH Neural Network Analysis Using Looser Isolated Tracks," CDF Note 10184.

[4] A. Buzatu, N. Krumnack, and A. Warburton, "Trigger Turnon Parametrizations for WH Search," CDF Note 9623.

[5] T. Chwalek *et al.*, "Update of the neural network b tagger for single-top analysis," CDF Note 8903.

[6] T. Aaltonen *et al.*, "Neural Network b-jet energy correction for WHNN analysis", CDF Note 9858.

[7] http://www.cs.toronto.edu/%7Eradford/fbm.software.html

[8] J. Adelman, T. Schwarz, J. Slaunwhite, et al. "Method II For You", CDF Note 9185

[9] http://www-cdf.fnal.gov/internal/physics/top/RunIIBtag/bTag.html

[10] http://www-cdf.fnal.gov/internal/physics/joint_physics/index.html

A Kinematic Distribution after Tagging

A.1 Kinematic Distributions after STST

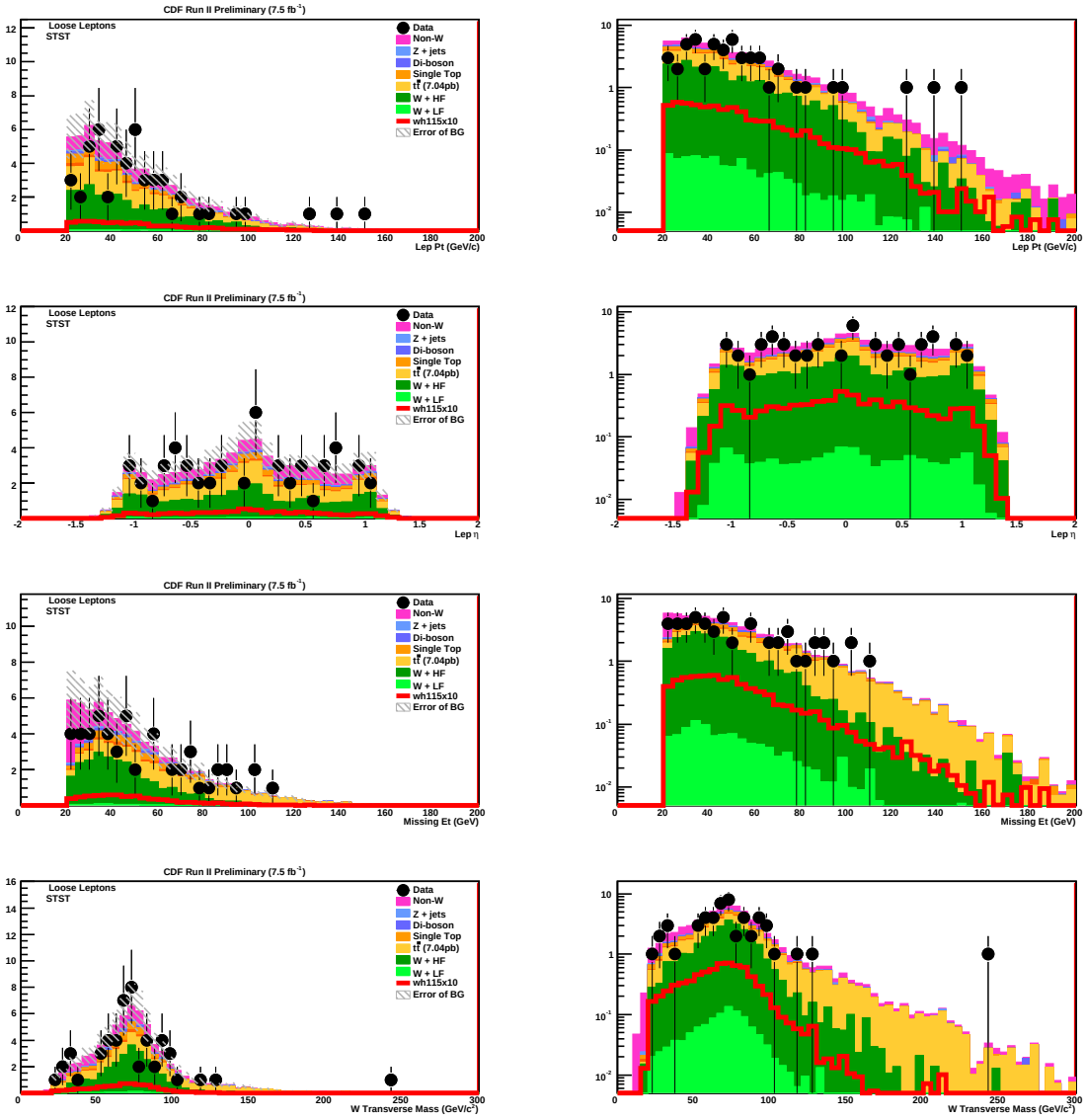

Figure 28: STST kinematic distributions for loose leptons: p_T, η,$\not\!\!E_T$, and W transverse mass.

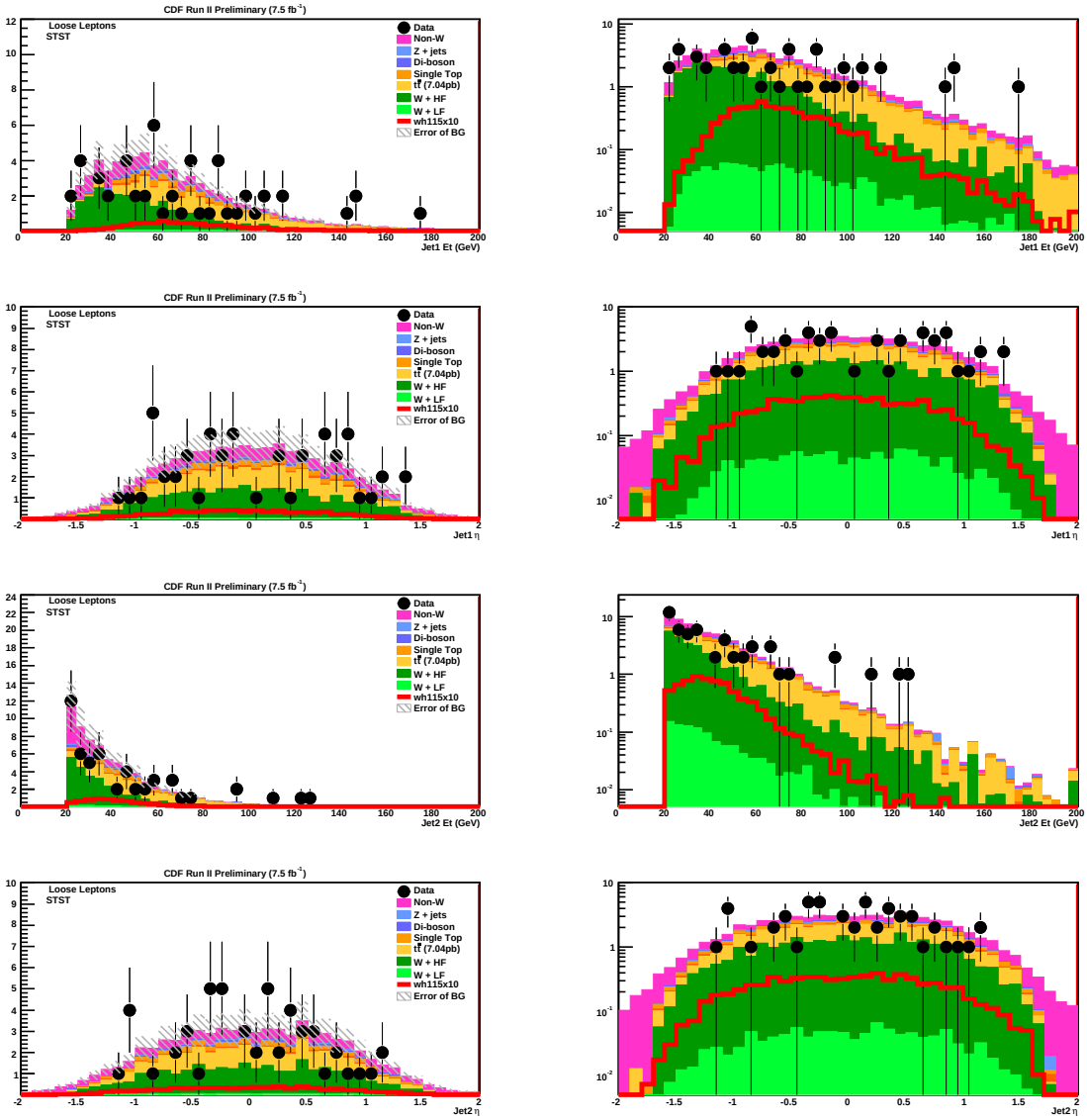

Figure 29: STST kinematic distributions for loose leptons: first jet E_T, η and second jet E_T, η.

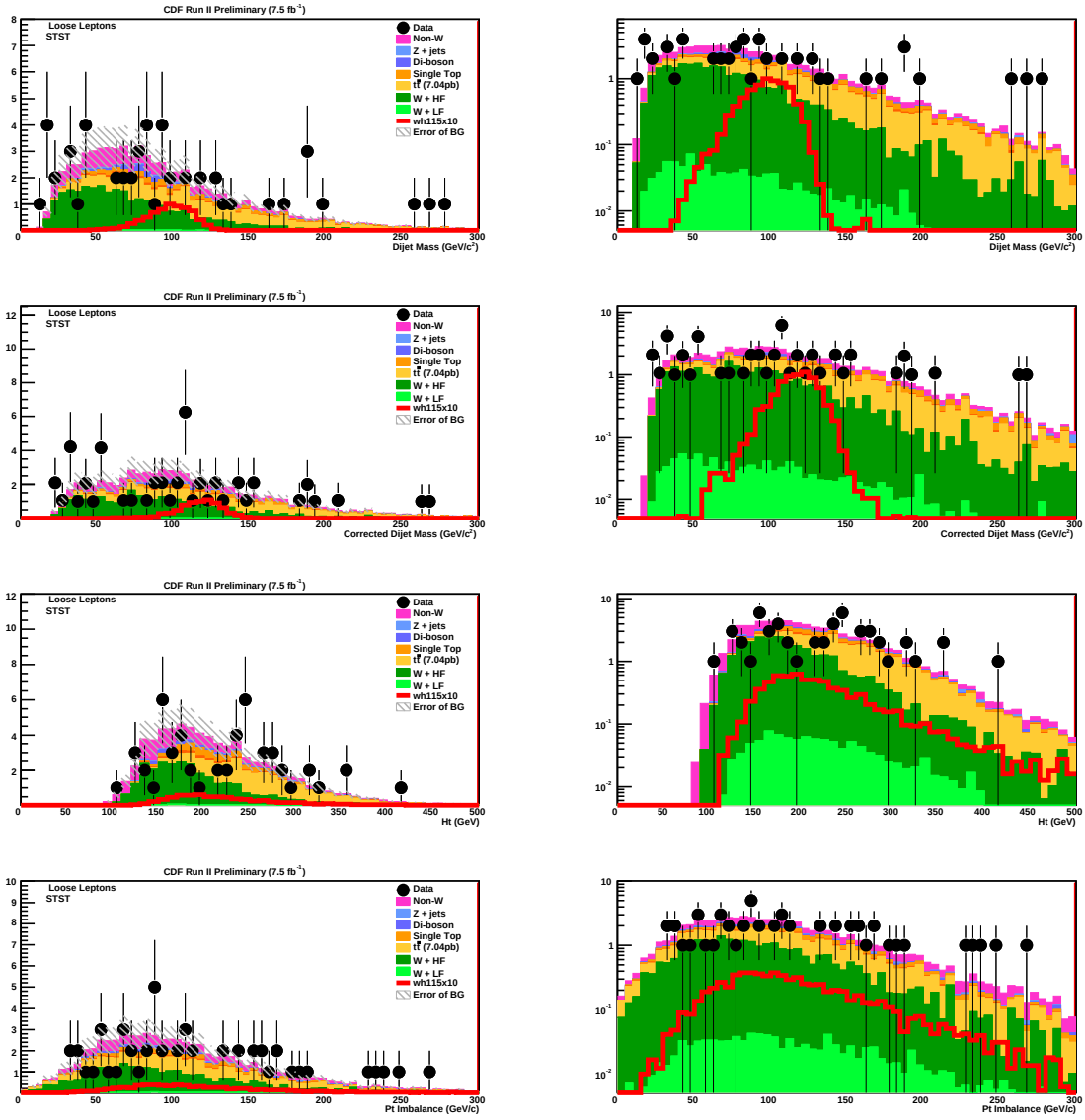

Figure 30: STST kinematic distributions for loose leptons: dijet mass before and after bjet energy correction, H_T, and P_T imbalance.

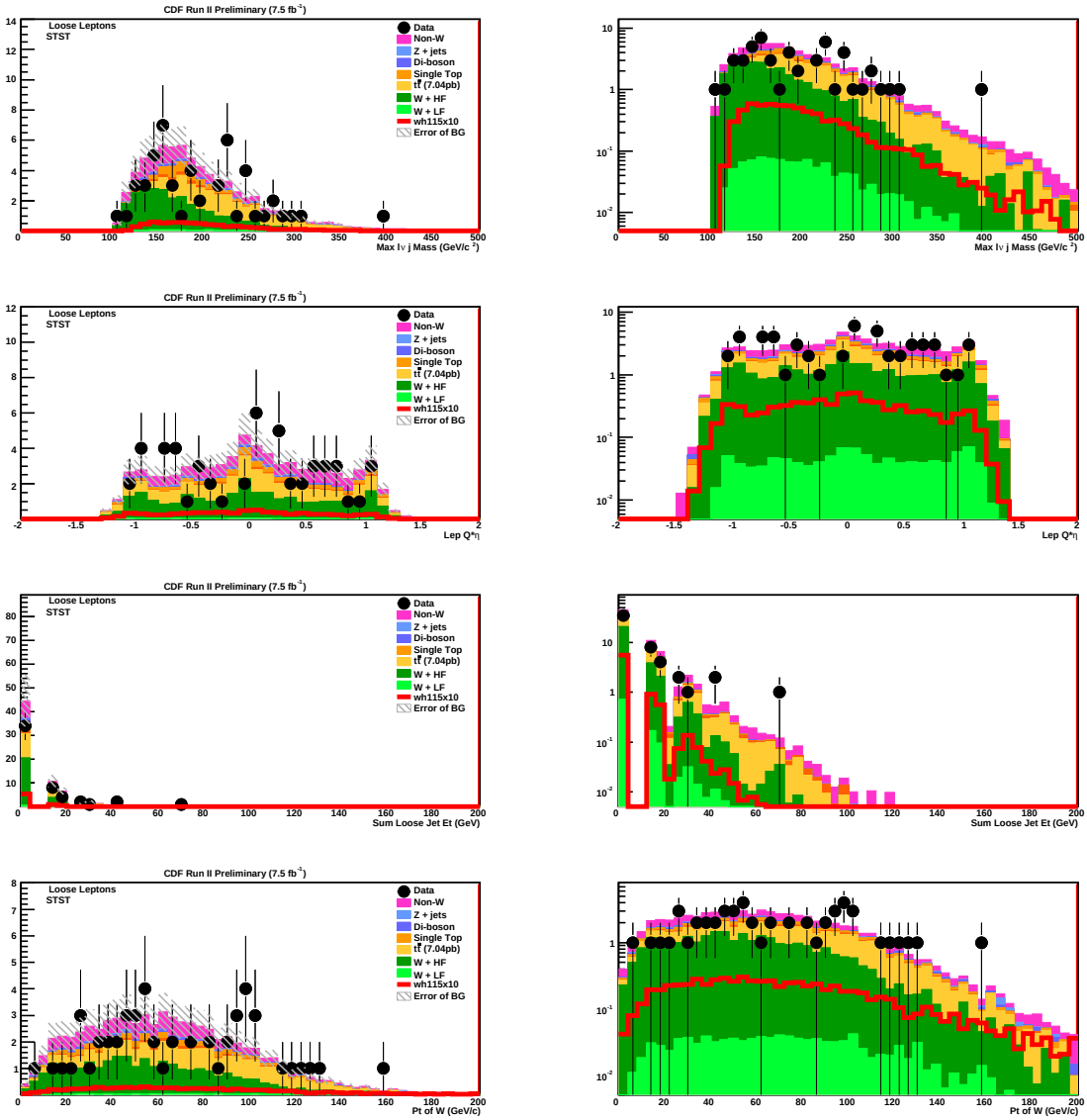

Figure 31: STST kinematic distributions for loose leptons: maximum of lvj mass, $\eta \times Q$, sum loose jet E_T, and P_T of W candidate.

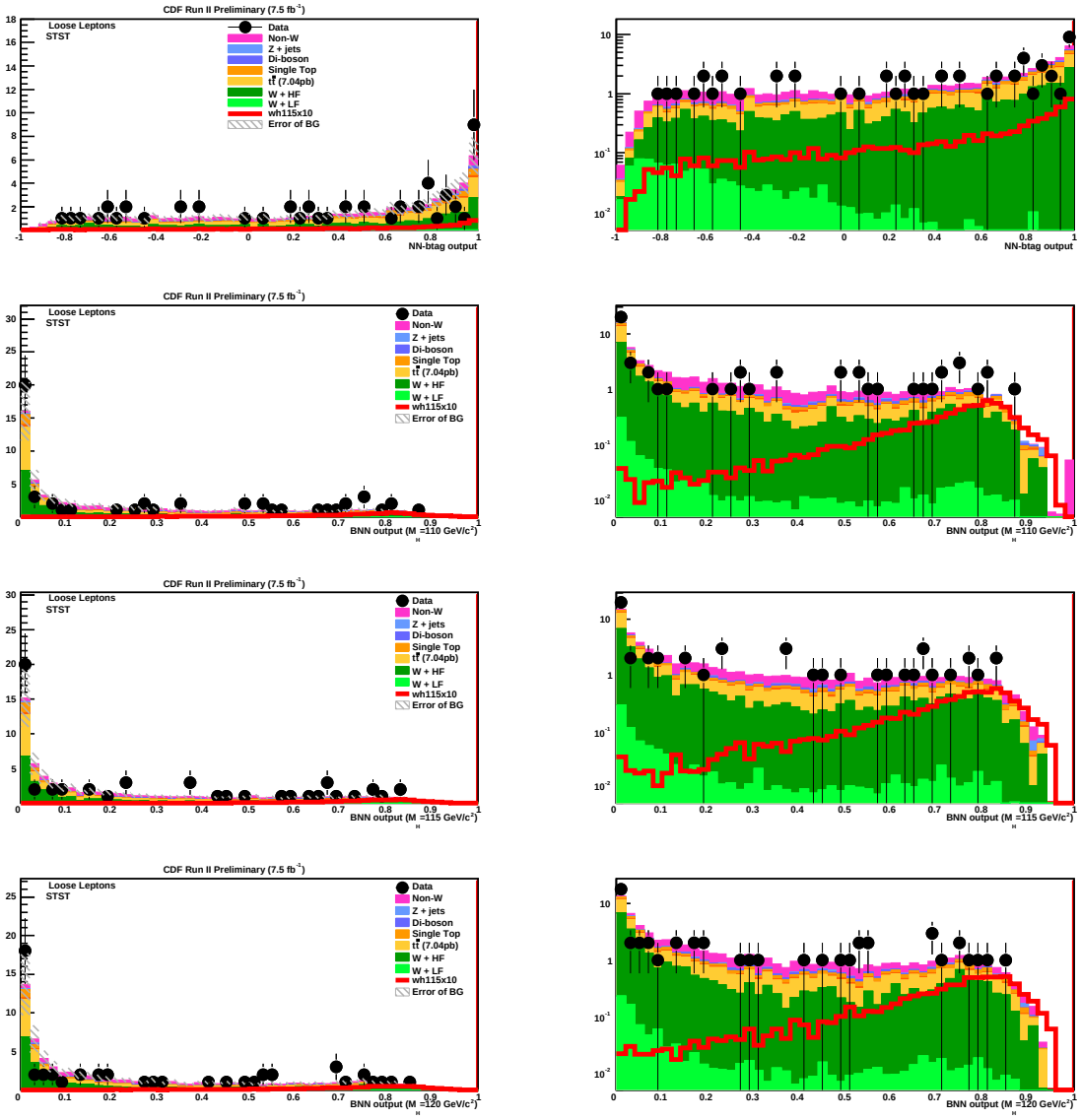

Figure 32: STST kinematic distributions for loose leptons: kitnn and Bnn output corresponds to m_H =110, 115, 120 GeV/c^2 respectively.

A.2 Kinematic Distributions after STJP

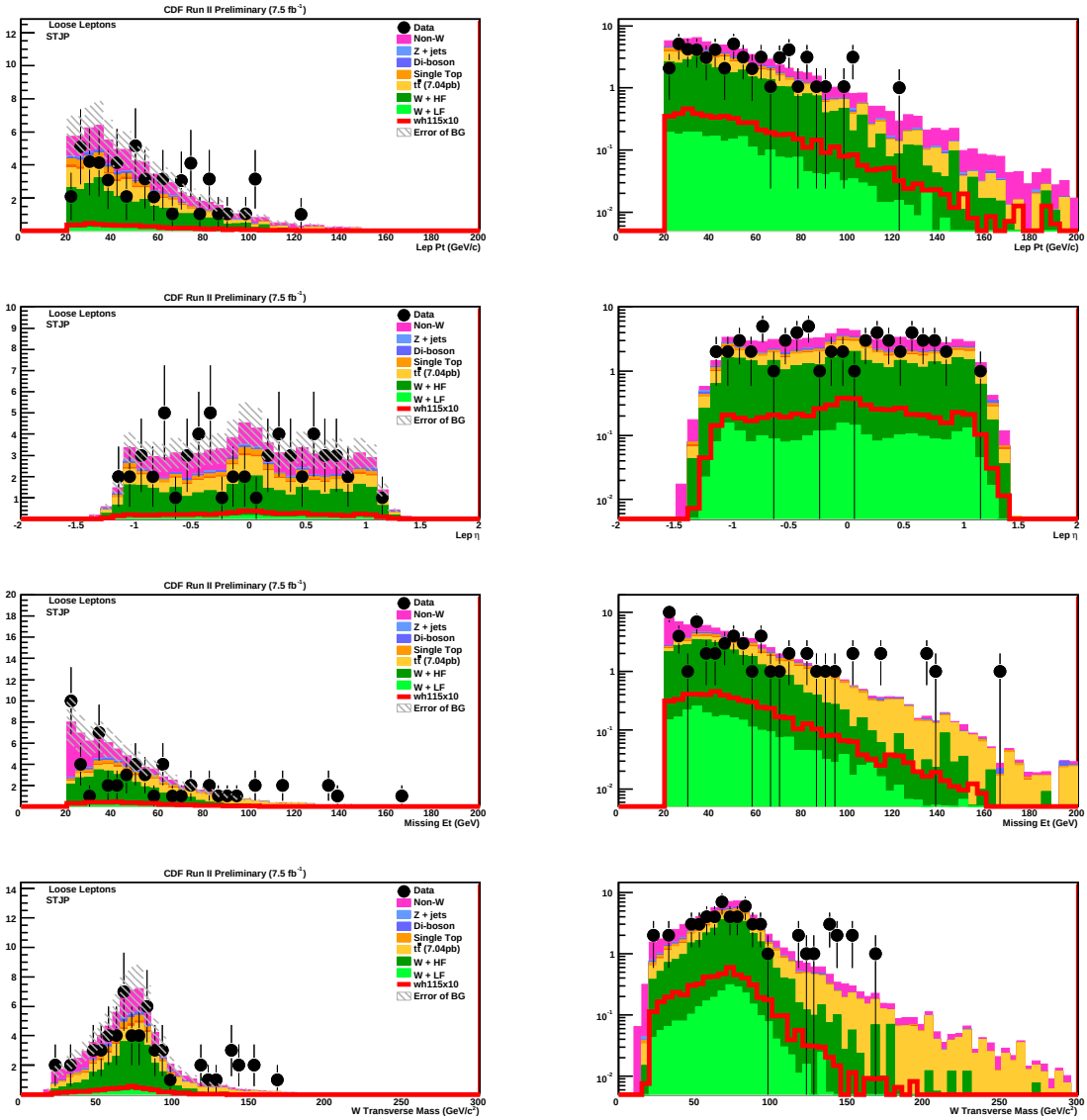

Figure 33: STJP kinematic distributions for loose leptons: p_T, η,$\not\!\!E_T$, and W transverse mass.

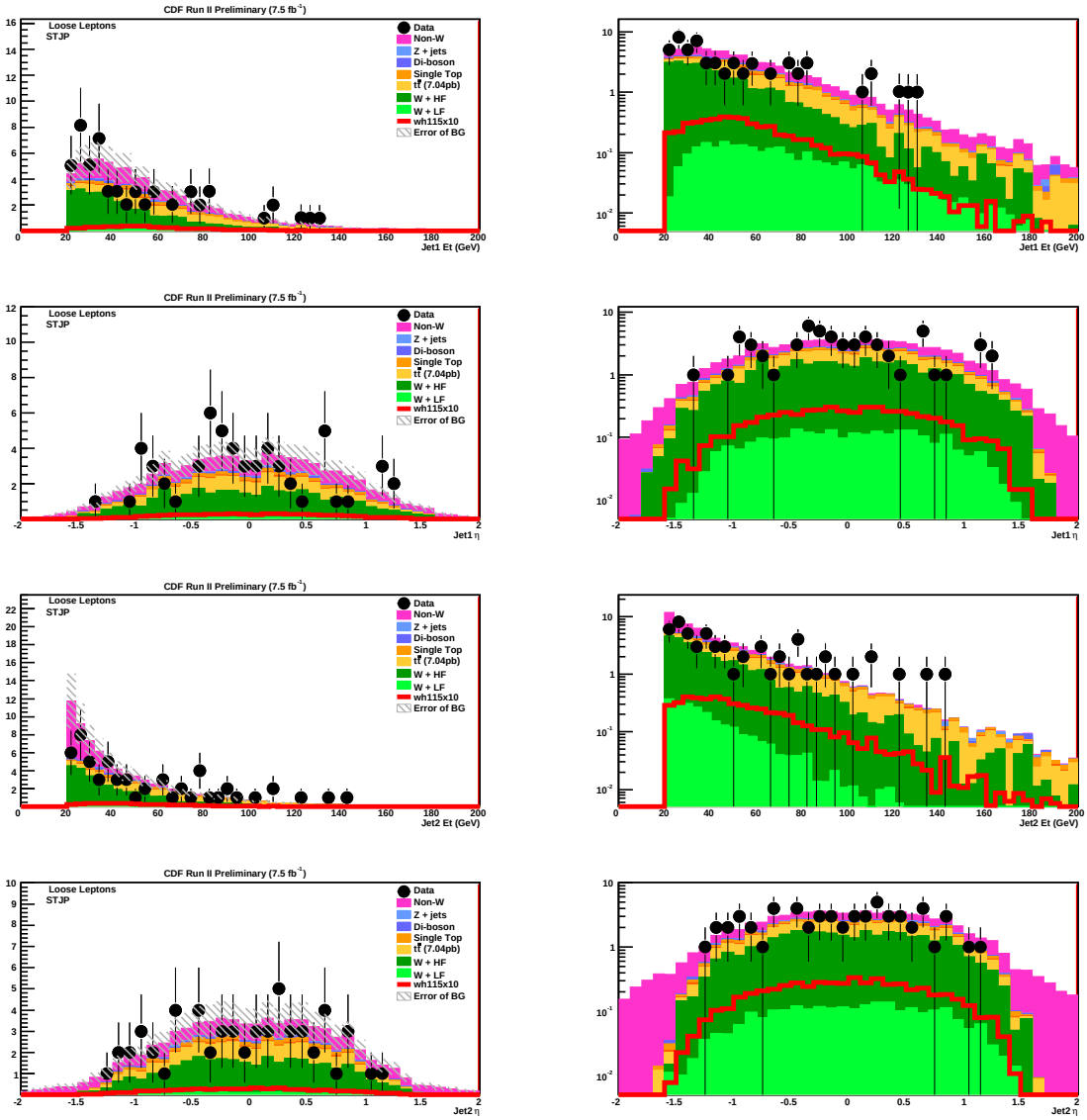

Figure 34: STJP kinematic distributions for loose leptons: first jet E_T, η and second jet E_T, η.

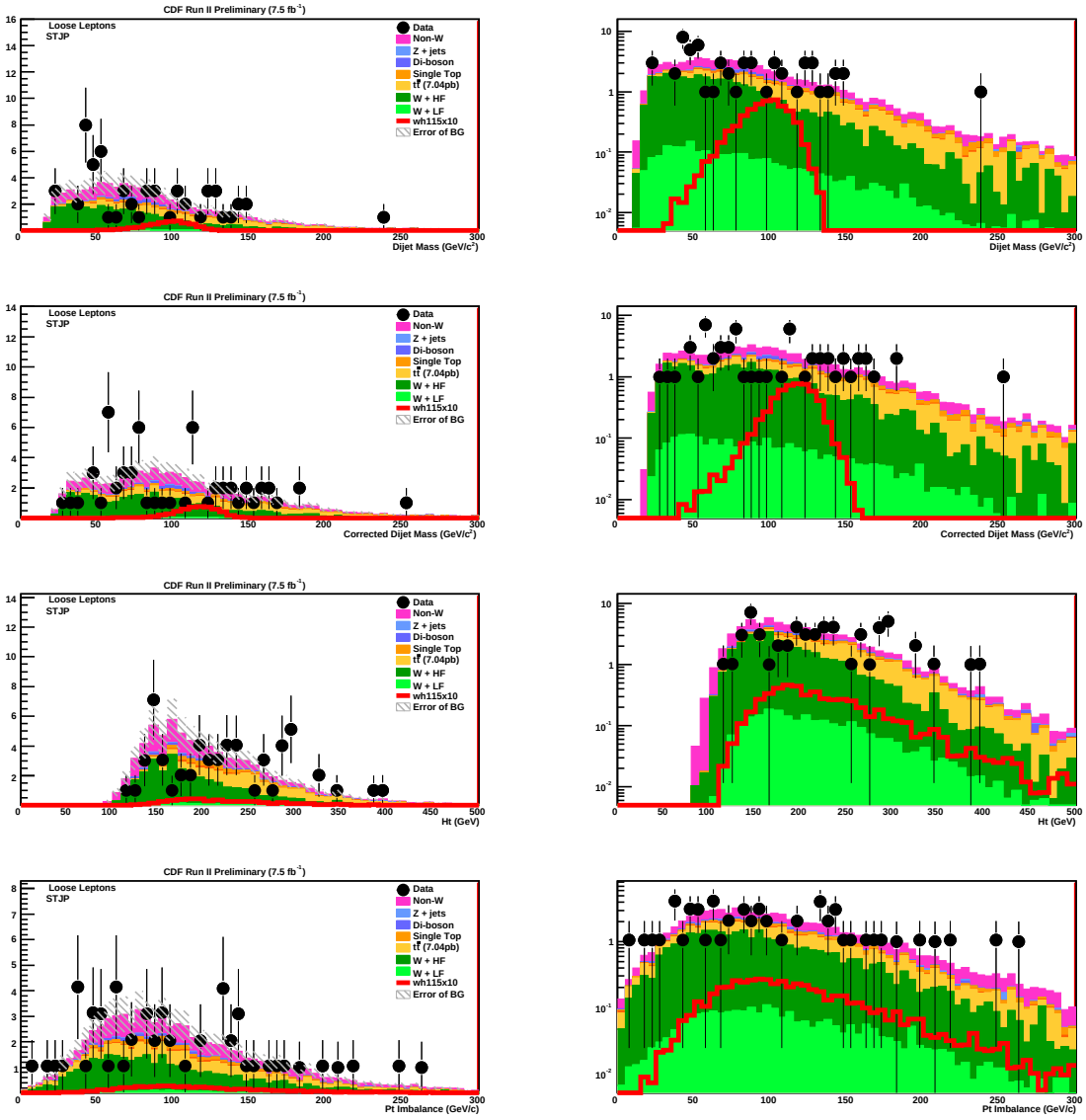

Figure 35: STJP kinematic distributions for loose leptons: dijet mass before and after bjet energy correction, H_T, and P_T imbalance.

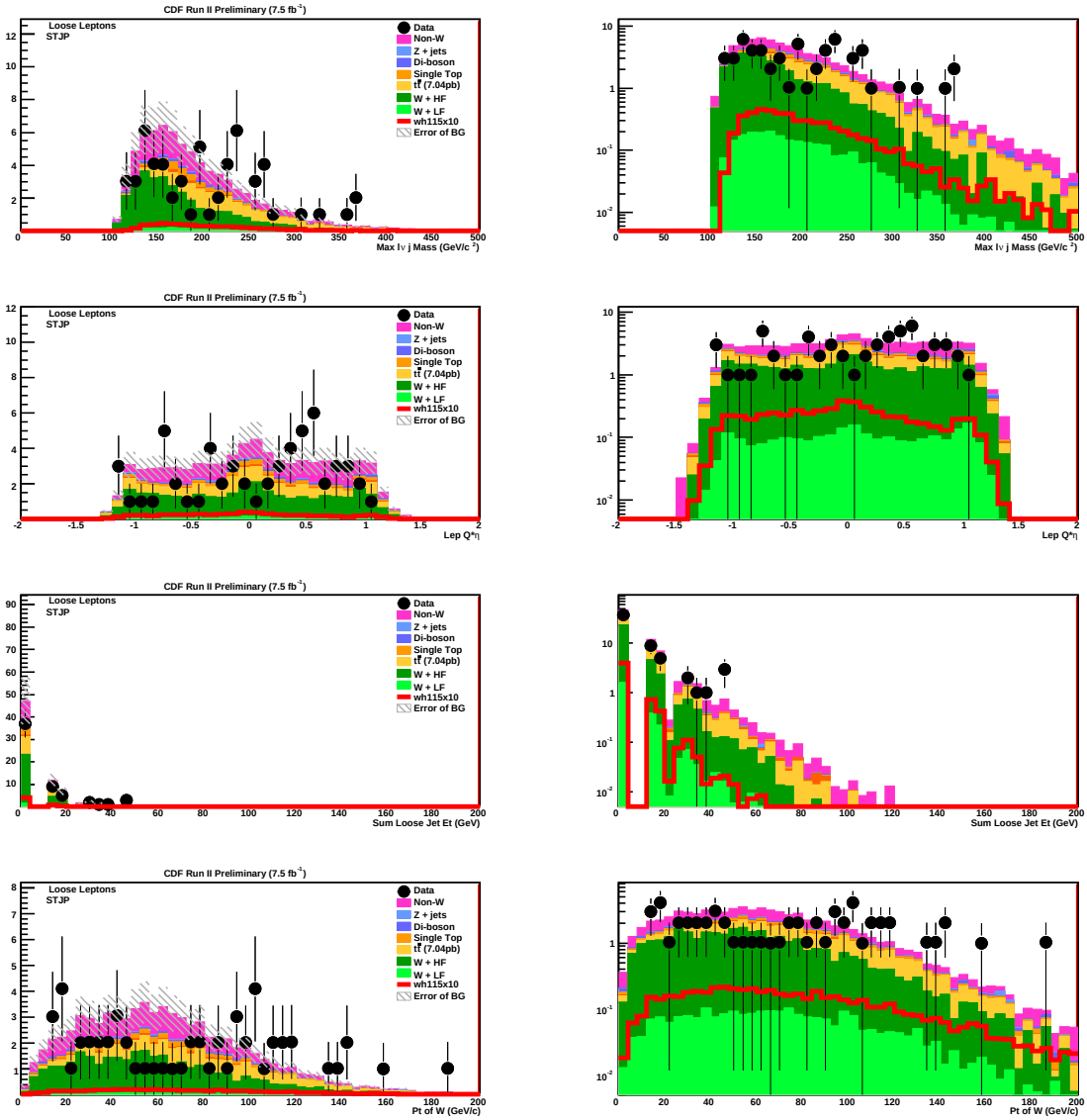

Figure 36: STJP kinematic distributions for loose leptons: maximum of lvj mass, $\eta \times Q$, sum loose jet E_T, and P_T of W candidate.

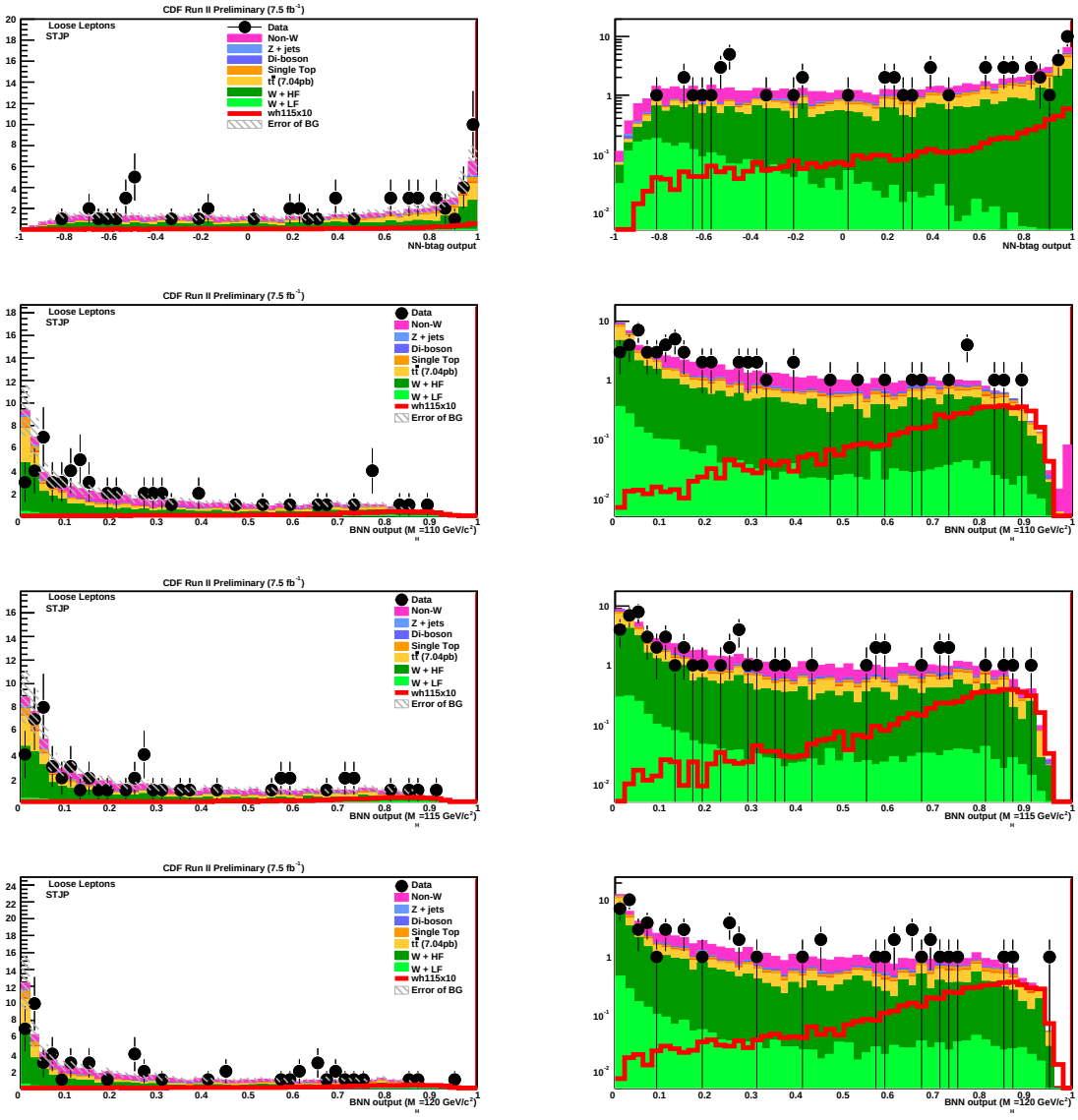

Figure 37: STJP kinematic distributions for loose leptons: kitnn and Bnn output corresponds to m_H =110, 115, 120 GeV/c^2 respectively.

A.3 Kinematic Distributions after STRoma

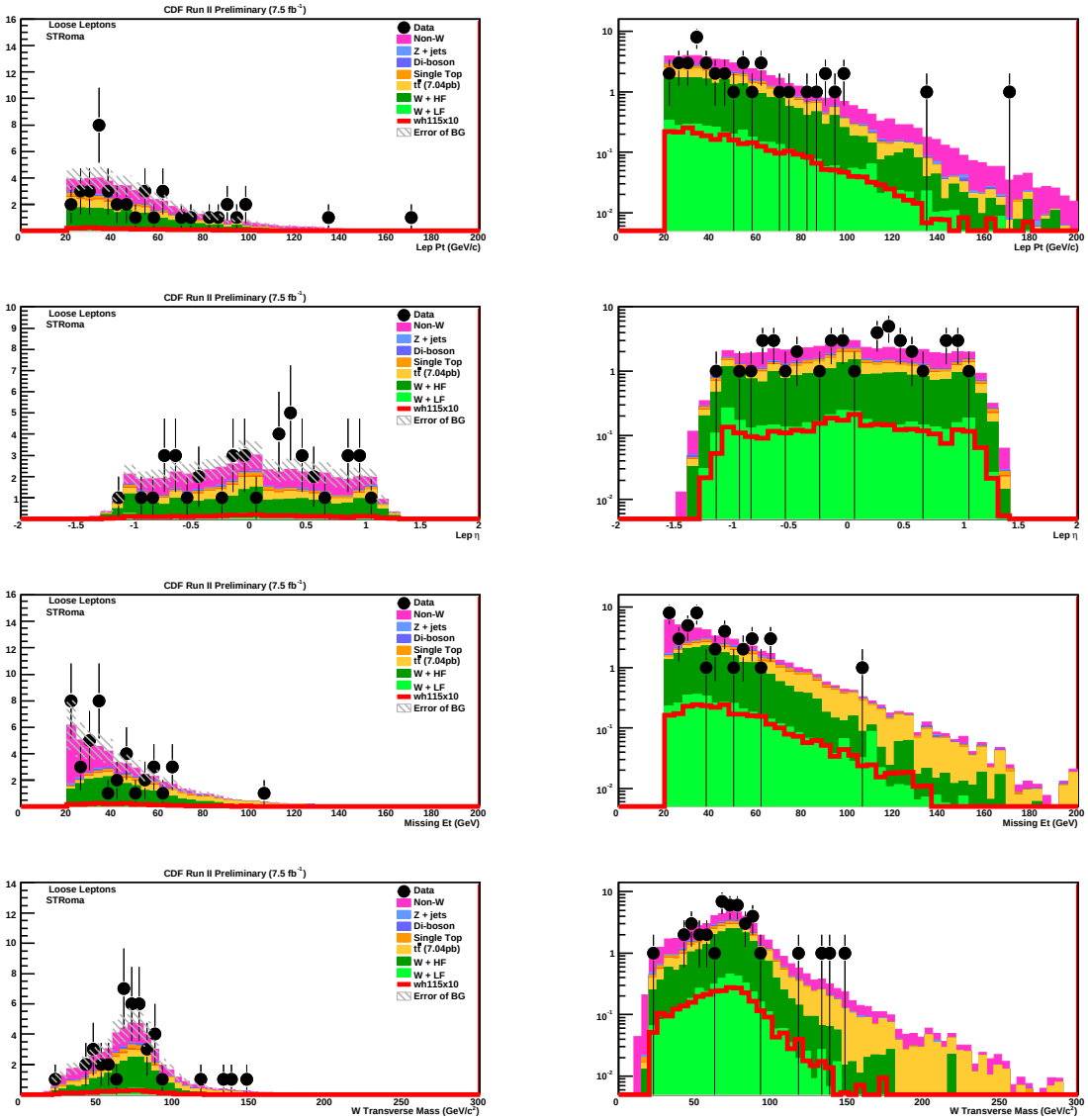

Figure 38: STRoma kinematic distributions for loose leptons: p_T, η,$\not\!\!E_T$, and W transverse mass.

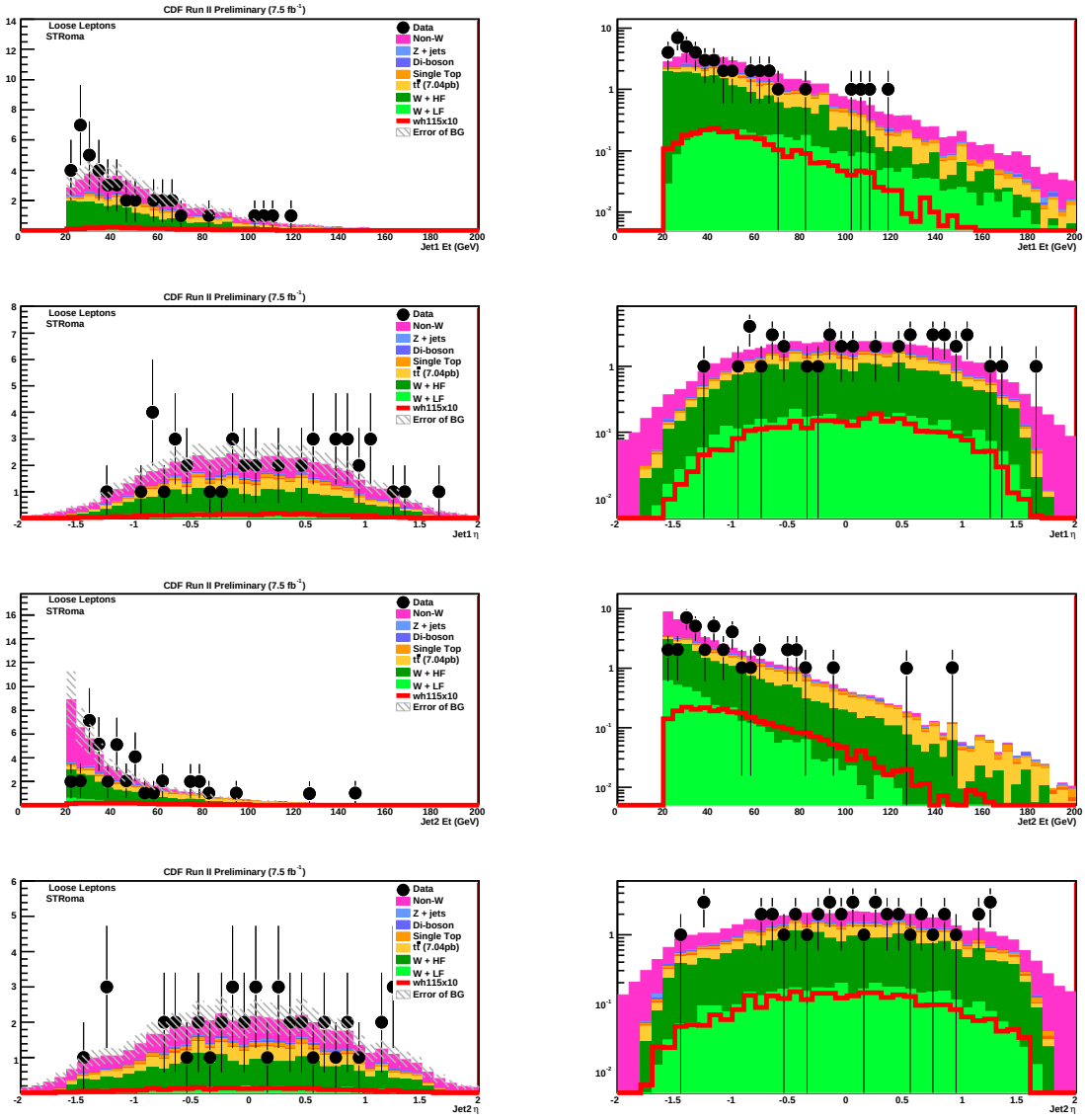

Figure 39: STRoma kinematic distributions for loose leptons: first jet E_T, η and second jet E_T, η.

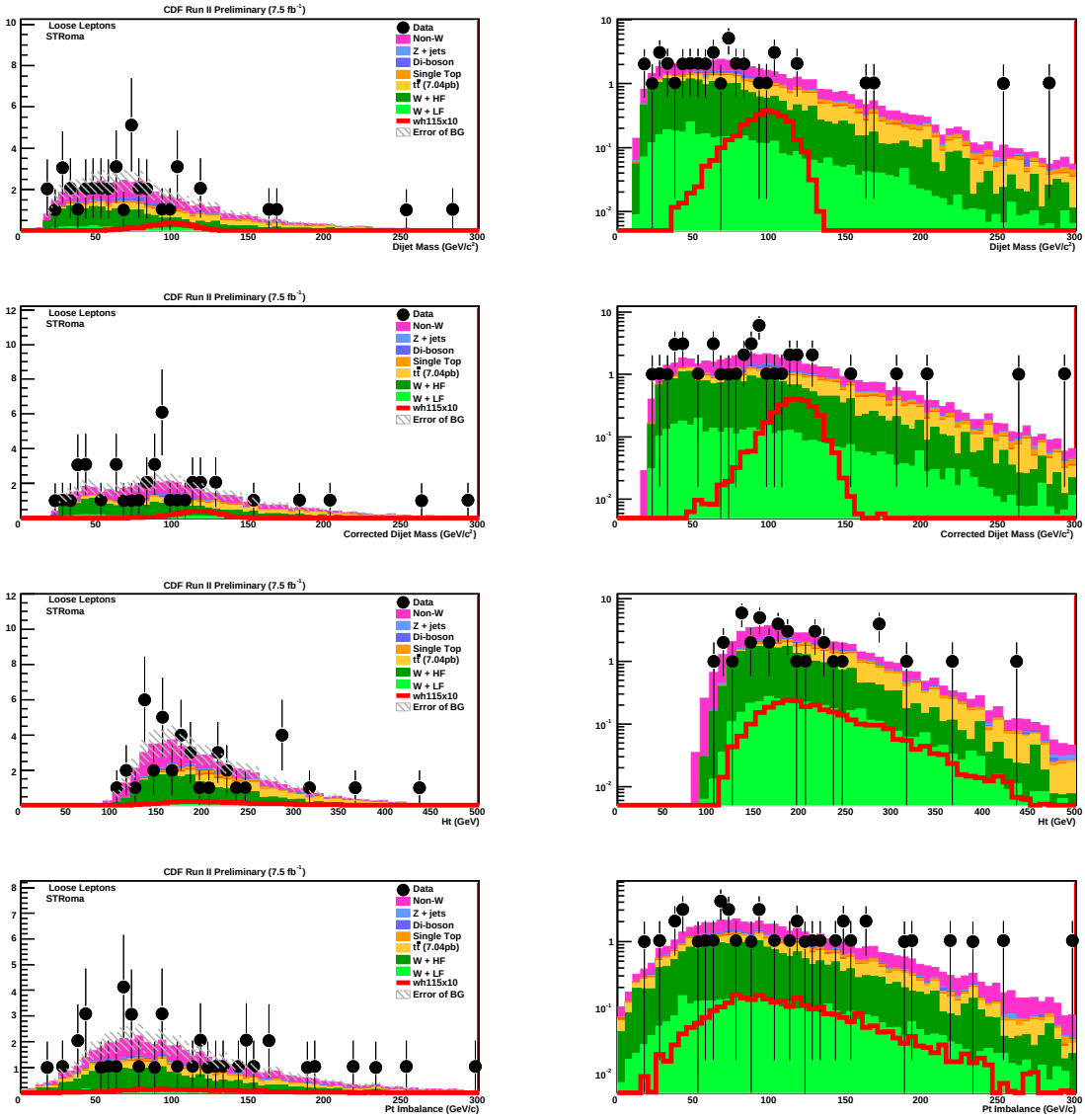

Figure 40: STRoma kinematic distributions for loose leptons: dijet mass before and after bjet energy correction, H_T, and P_T imbalance.

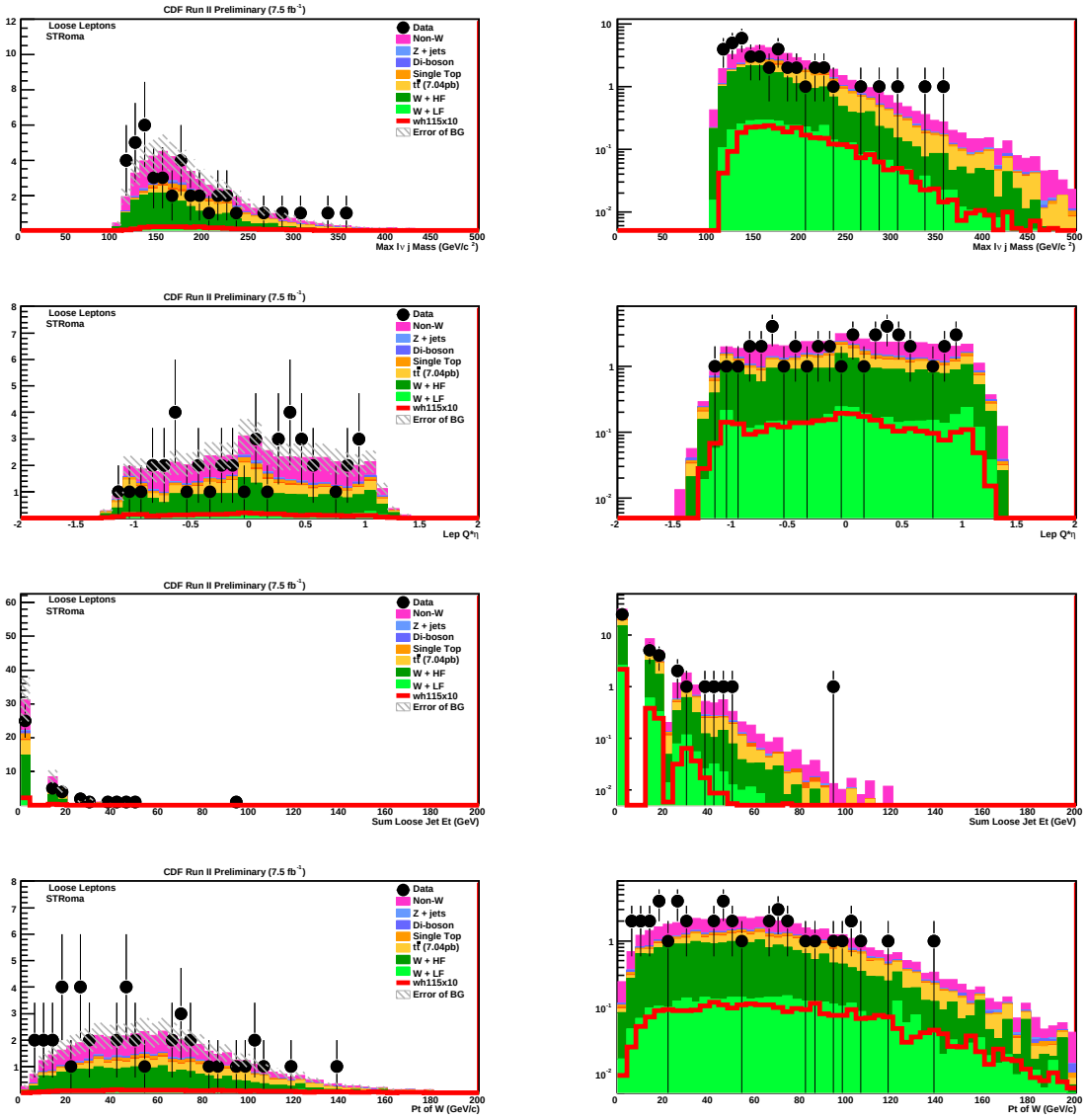

Figure 41: STRoma kinematic distributions for loose leptons: maximum of lvj mass, $\eta \times Q$, sum loose jet E_T, and P_T of W candidate.

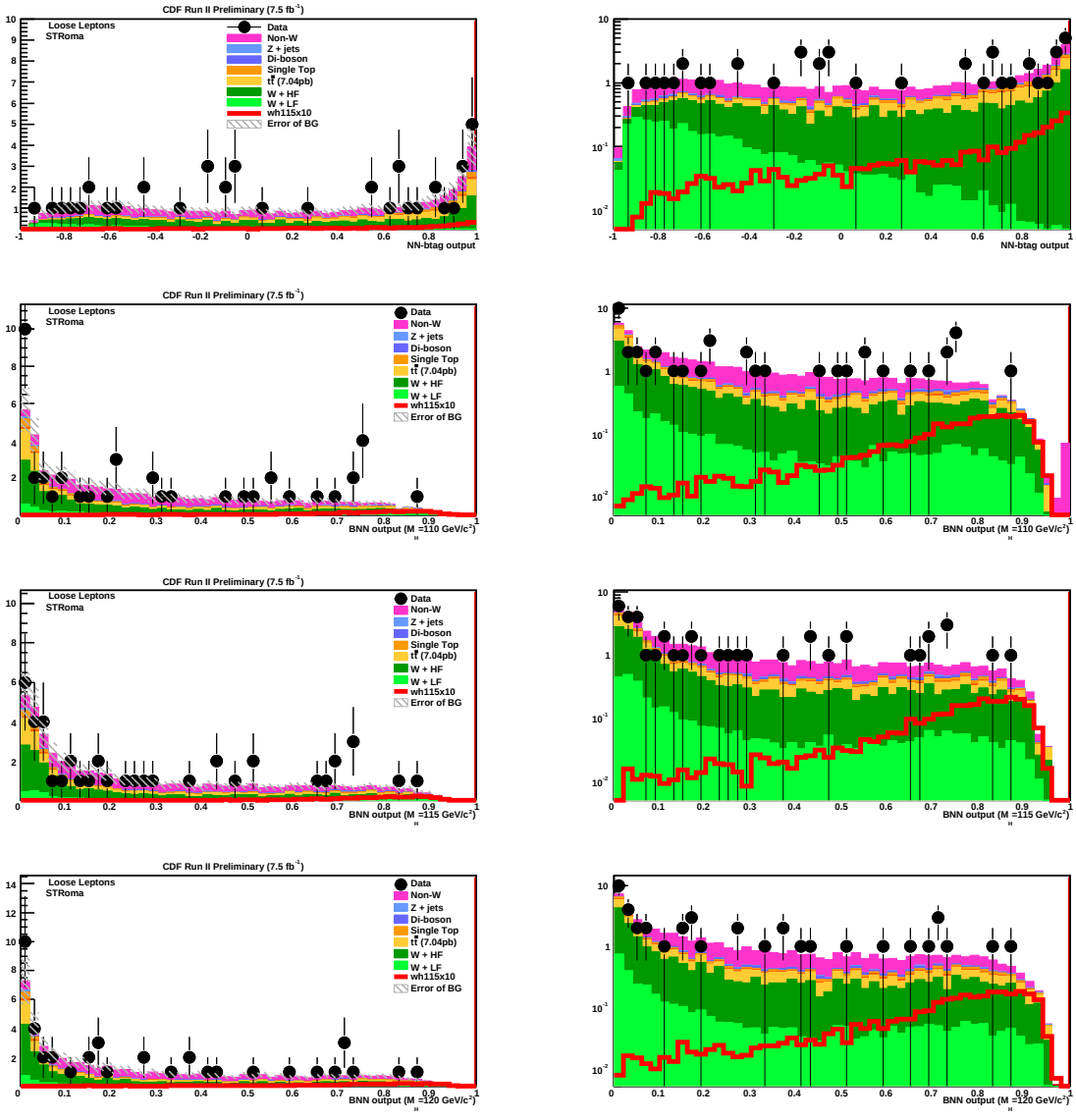

Figure 42: STRoma kinematic distributions for loose leptons: kitnn and Bnn output corresponds to m_H =110, 115, 120 GeV/c^2 respectively.

A.4 Kinematic Distributions after SST

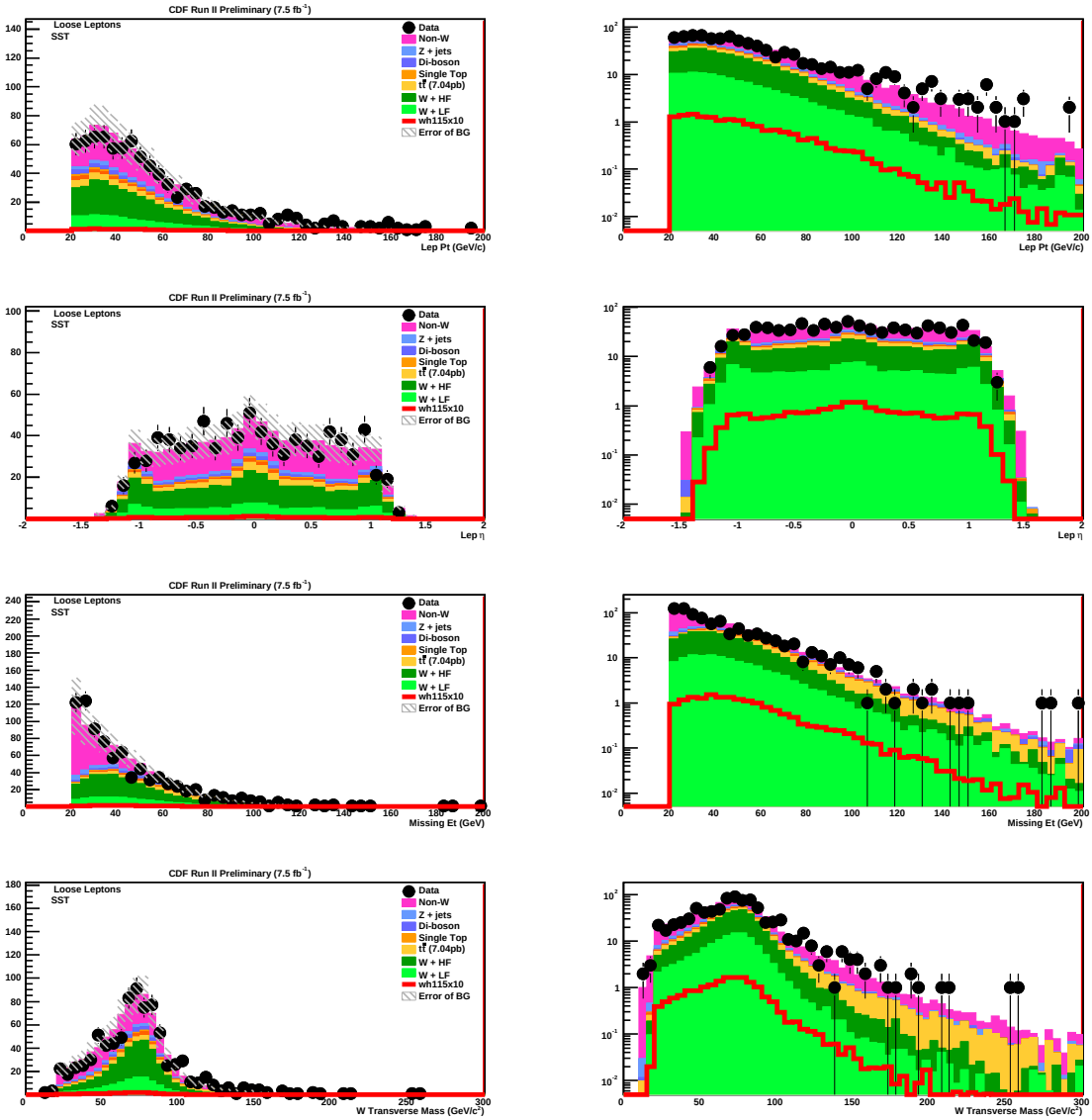

Figure 43: SST kinematic distributions for loose leptons: p_T, η,$\not\!\!E_T$, and W transverse mass.

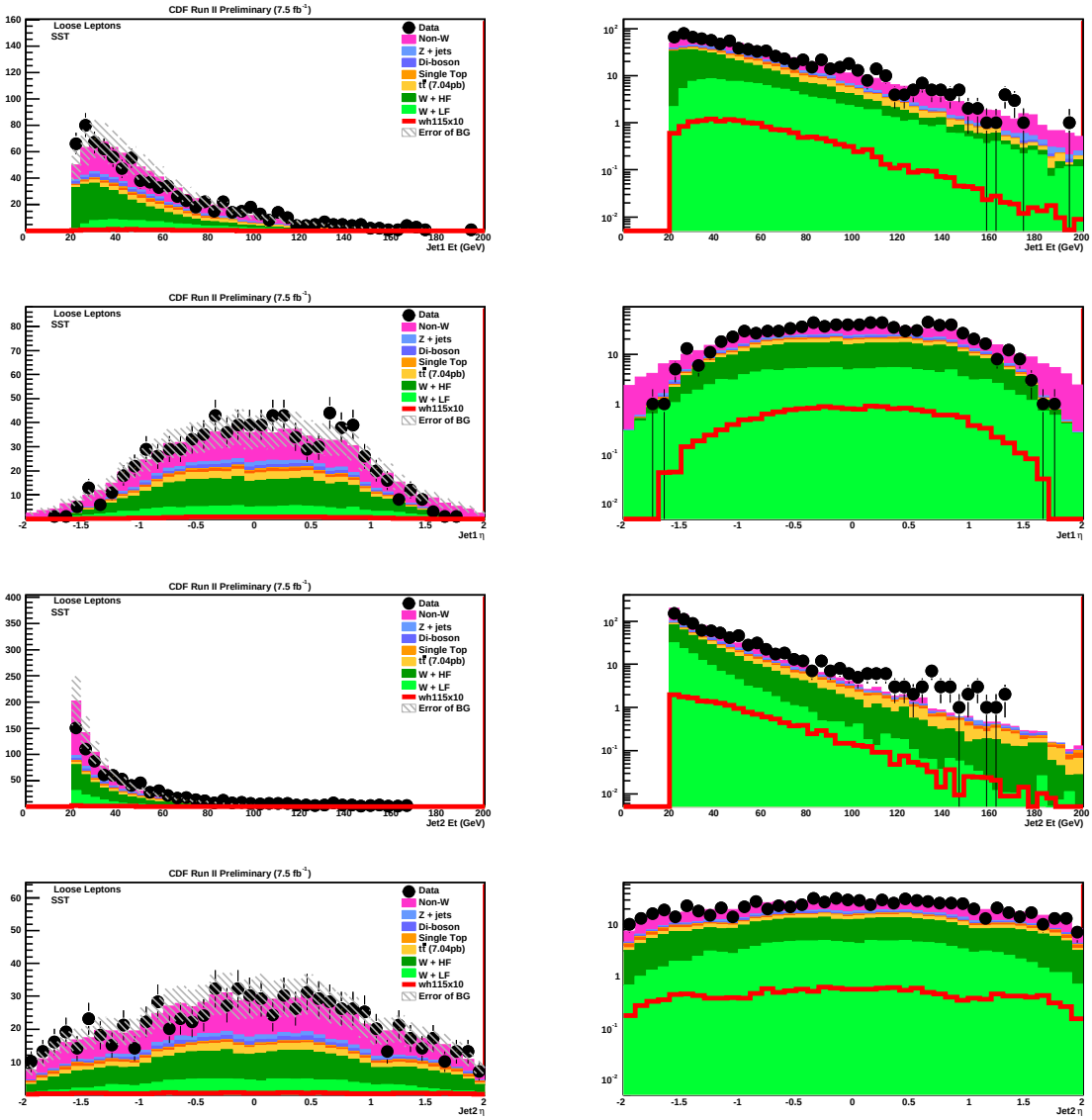

Figure 44: SST kinematic distributions for loose leptons: first jet E_T, η and second jet E_T, η.

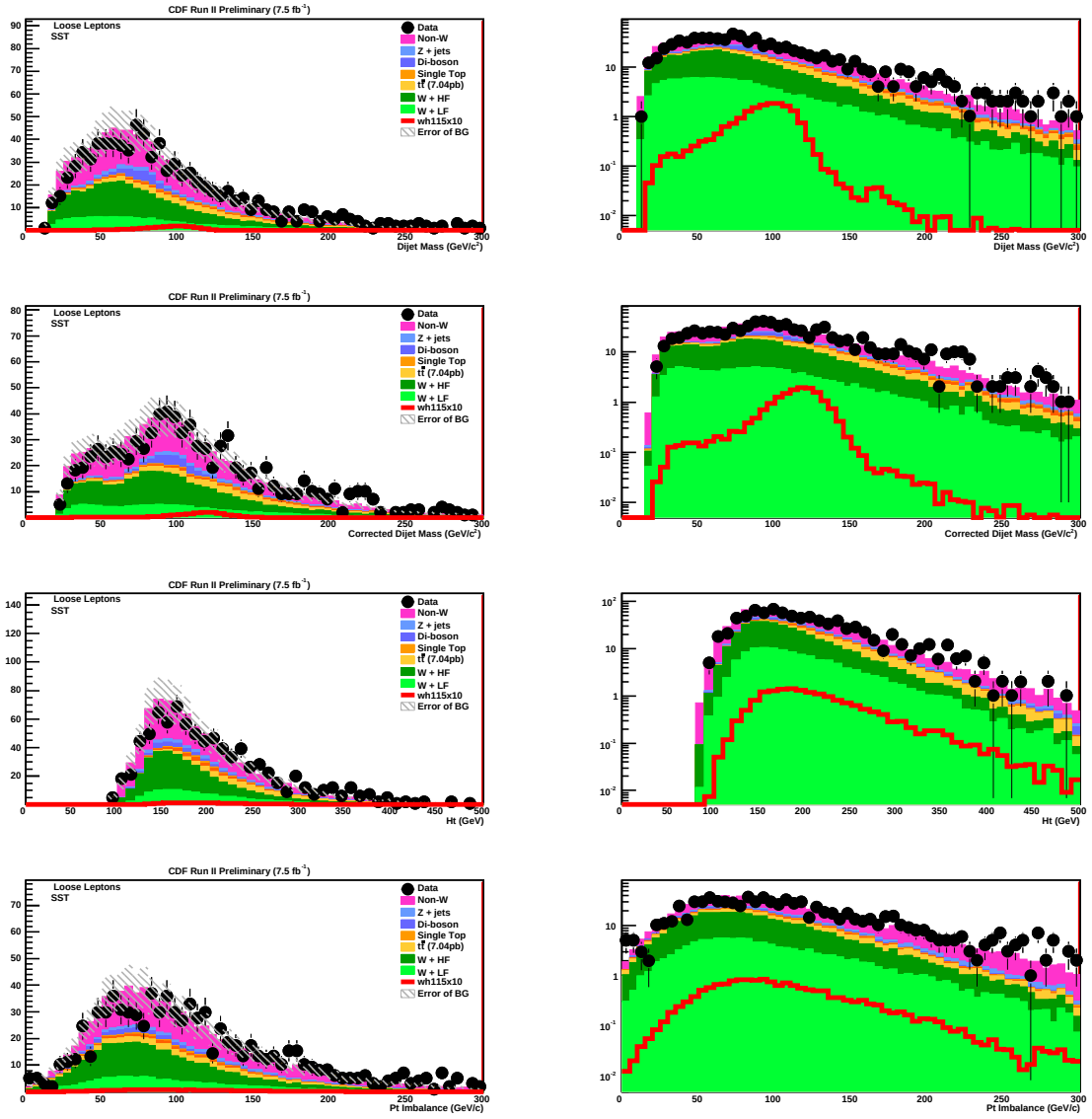

Figure 45: SST kinematic distributions for loose leptons: dijet mass before and after bjet energy correction, H_T, and P_T imbalance.

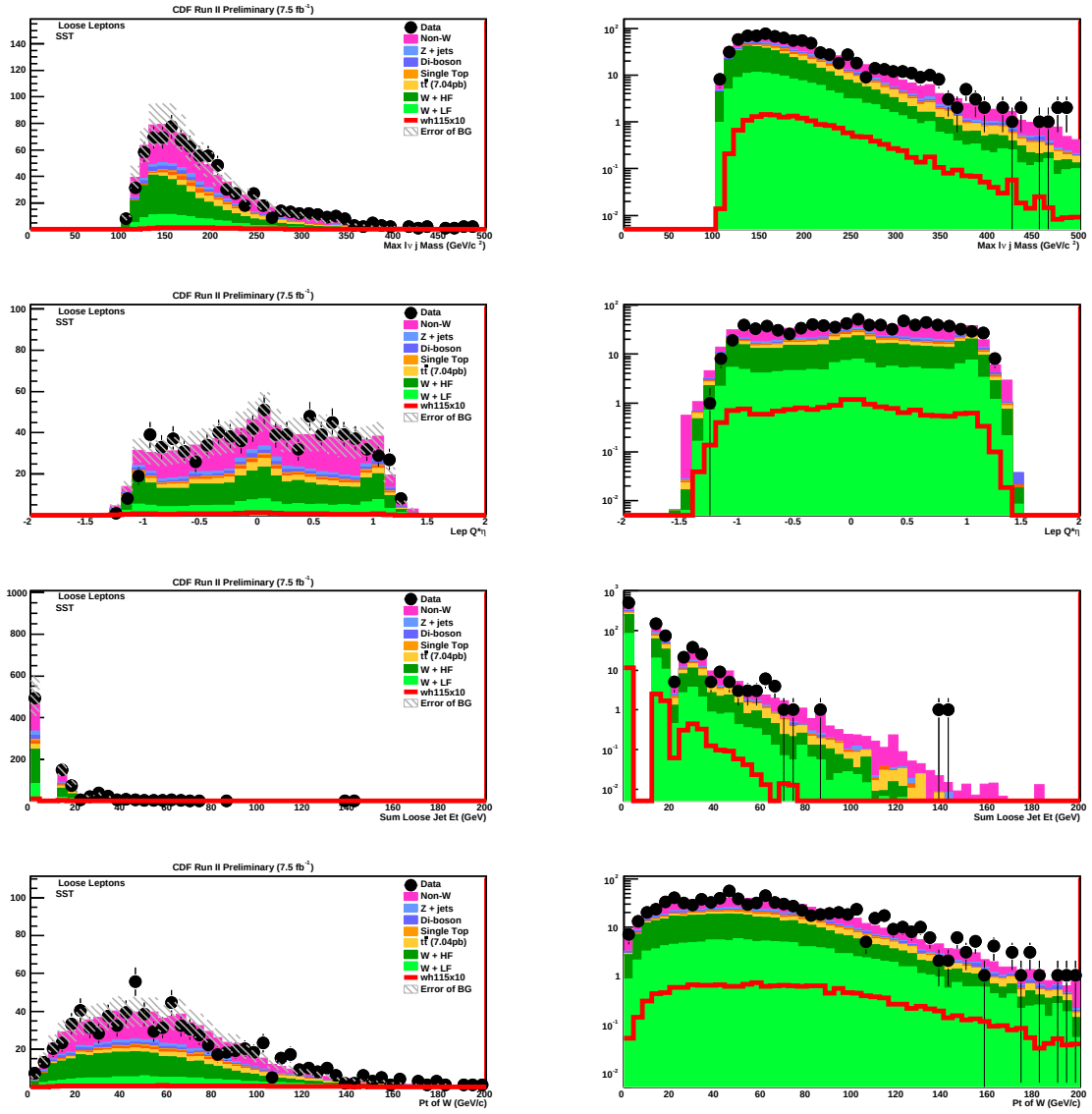

Figure 46: SST kinematic distributions for loose leptons: maximum of lvj mass, $\eta \times Q$, sum loose jet E_T, and P_T of W candidate.

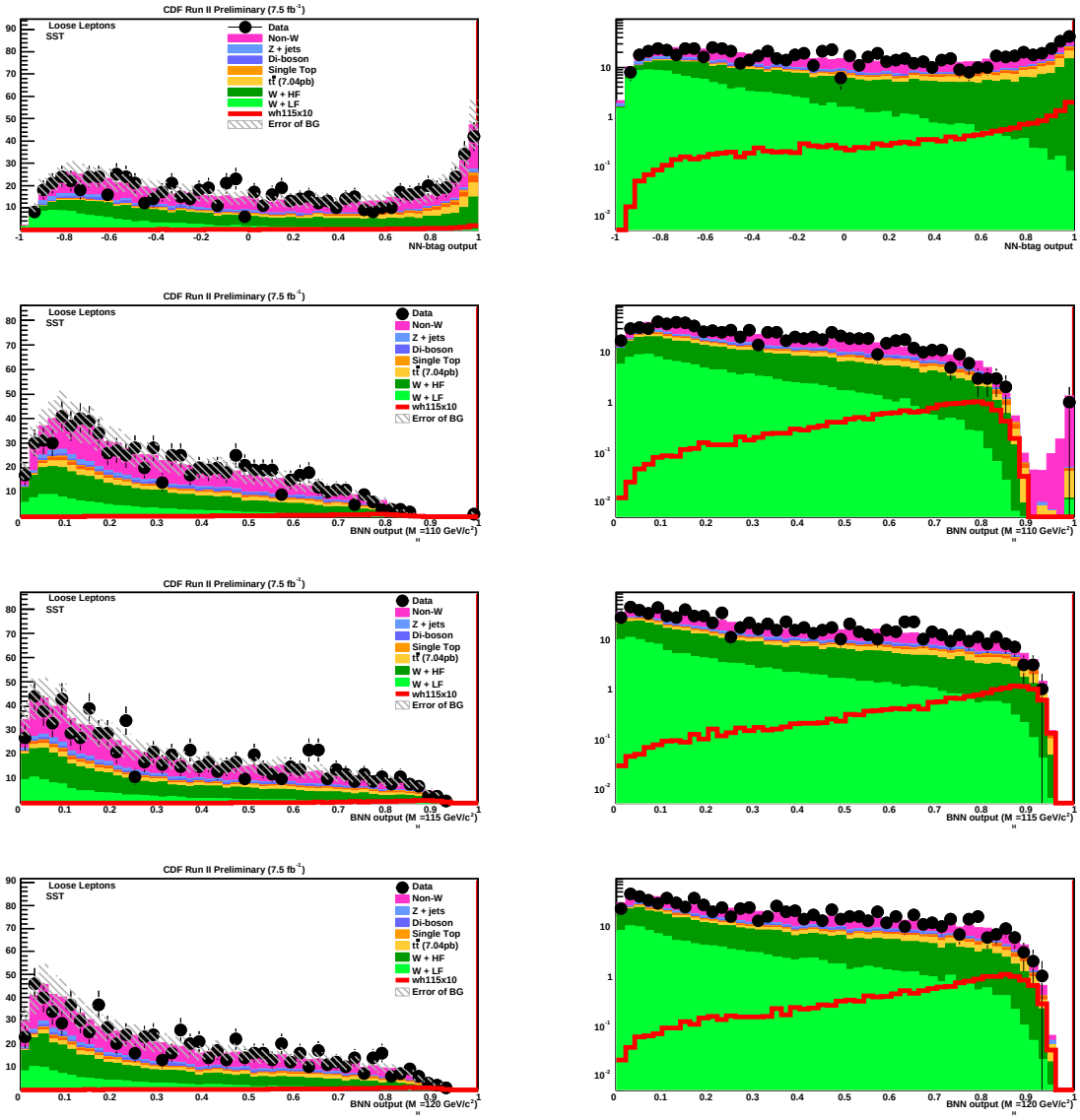

Figure 47: SST kinematic distributions for loose leptons: kitnn and Bnn output corresponds to m_H =110, 115, 120 GeV/c^2 respectively.